

# FAULT ANALYSIS OF SINGLE WALLED CARBON NANOTUBE

## A DISSERTATION

*Submitted in partial fulfillment of the requirements for the award of the degree*

*of*

MASTER OF TECHNOLOGY

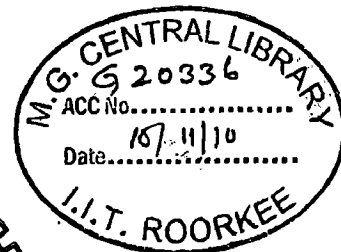
*in*

MECHANICAL ENGINEERING

(With Specialization in Machine Design Engineering)

*By*

**AASHISH BHATNAGAR**



DEPARTMENT OF MECHANICAL AND INDUSTRIAL ENGINEERING  
INDIAN INSTITUTE OF TECHNOLOGY ROORKEE  
ROORKEE-247 667 (INDIA)

JUNE, 2010

## CANDIDATE'S DECLARATION

---

I hereby declare that the work carried out in this dissertation report entitled

### “FAULT ANALYSIS OF SINGLE WALLED CARBON NANOTUBE”

is presented on behalf of partial fulfilment of the requirements for the award of degree of “Master of Technology” in Mechanical Engineering with specialization in Machine Design submitted to the Department of Mechanical and Industrial Engineering, Indian Institute of Technology, Roorkee under the supervision of Dr. S.C. Sharma, Professor & HOD and Dr. S.P. Harsha, Assistant Professor, Department of Mechanical and Industrial Engineering.

I have not submitted the record embodied in this report for the award of any other degree or diploma.

Date: 28-06-2010

Place: Roorkee

  
AASHISH BHATNAGAR

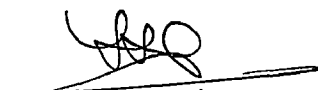
## CERTIFICATE

---

This is to certify that the above statement made by the candidate is correct to the best of my knowledge and belief.


Date: 28-06-2010

Place: Roorkee

  
28/06/10  
Dr. S. C. Sharma

Professor & HOD

MIED IIT Roorkee

  
Dr.S.P.Harsha

Assistant Professor

MIED IIT Roorkee

## ACKNOWLEDGEMENT

---

I wish to express an immense pleasure and sincere thanks to **Dr. S.P. Harsha**, Assistant Professor and **Dr. S.C.Sharma** Professor & HOD, in the Department of Mechanical & Industrial Engineering, IIT Roorkee for their valuable guidance and support. This work is simply the reflection of their thoughts, ideas and concepts and about their efforts. Working under their guidance was a privilege and an excellent learning experience that I will cherish for life time.

I am especially thankful to **Mr. Anand Y Joshi** for giving me directions and sharing new ideas throughout my dissertation work. I am very thankful to **Mr. P.K. Kankar** for their encouragement and support.

I am very thankful to my parents, my fiancées and all of my friends for their never ending encouragement in bringing out this dissertation report to the form which it is in now. This work would have not been possible without their belief in me and their endless support.

Date: 28-06-2010.

Place: Roorkee

**AASHISH BHATNAGAR**

## ABSTRACT

---

Since the discovery of Carbon Nanotubes (CNT) they have been a subject of extensive research. Carbon nanotubes are the strongest and stiffest materials yet discovered in terms of tensile strength and elastic modulus respectively. The strength and flexibility of carbon nanotubes makes them of potential use in controlling other nanoscale structures that is why they play an important role in nanotechnology engineering. Carbon Nanotube are been used as potential application component as resonators, mass sensor and structural element in mechanical field. Some of these applications require high amount of precision in measurement and CNT to be faultless. But due to the inherent defects in Carbon Nanotube actual properties of CNT differ and are difficult to simulate.

In this report the effect of defects on the vibration behaviour of Carbon Nanotube is discussed in detail. The extent of this report is limited to the analytical and numerical analysis of defects in Single walled Carbon Nano Tube (SWCNT). Effect of various CNT parameters like length, diameter and chirality has been illustrated. Different type of defects are analysed based on their role in application of CNT. In case of application of CNT as nanotube based resonator and mass sensors, defects that are taken into consideration are waviness, vacancy defect and pinhole defect. In case of CNT application as a structural element, the effect of loading on crack propagation is studied. Outcome of this report helps us to predict the change in properties of CNT like resonant frequency due to various defects and how CNT parameters affect the vibrational behaviour. Simulation results can also be used to predict the pattern in crack propagation under tensile loading.

# TABLE OF CONTENTS

---

<b>TITLE</b>	<b>PAGE NO</b>
CANDIDATE DECLARATION	i
ACHNOLOWDGEMENT	ii
ABSTRACT	iii
LIST OF FIGURES	vii
LIST OF TABLE	xi
NOMENCLATURE	xii
<b>CHAPTER 1 – INRODUCTION</b>	<b>1</b>
1.1 INTRODUCTION	2
1.2 OBJECTIVE OF DISSERTATION	2
1.3 OUTLINE OF DISSERTATION	3
<b>CHAPTER 2 – CARBON NANOTUBES</b>	<b>4</b>
2.1 CNT STRUCTURE	5
2.1.1 SINGLE WALLED NANOTUBES	5
2.1.2 MULTIWALLED NANOTUBES	8
2.2 CNT FABRICATION TECHNIQUES	9
2.2.1 CHEMICAL VAPOUR DEPOSITION	9
2.2.2 ARC DISCHARGE	10
2.2.3 LASER ABLATION	11
2.3 CNT MECHANICAL PROPERTIES	12
2.4 APPLICATIONS OF CARBON NANOTUBES	13
2.4.1 CARBON NANOTUBE COMPOSITES	14
2.4.2 SENSORS AND PROBES	14

<b>CHAPTER 3 - DEFECTS IN NANOTUBE</b>	16
3.1 STONE WALLS DEFECTS	18
3.2 WAVINESS IN THE CNT	19
3.3 VACANCY DEFECT	20
3.4 PINHOLE DEFECT	21
3.5 FRACTURES IN CNT	22
<b>CHAPTER 4 - MODELLING AND SIMULATION</b>	24
4.1 MODELLING & SIMULATION TECHNIQUES	25
4.1.1 MOLECULAR DYNAMICS	25
4.1.2 STRUCTURAL MECHANICS	26
4.1.3 DISSIPATIVE PARTICLE DYNAMICS	26
4.1.4 CONTINUUM MECHANICS	27
4.1.5 OTHER SIMULATION METHODS	27
4.2 MODELLING AND SIMULATION PARAMETERS	28
4.2.1 CONTINUUM MECHANICS	28
4.2.2 STRUCTURAL MECHANICS	29
<b>CHAPTER 5 - NANOMECHANICAL RESONATORS</b>	31
5.1 ANALYTICAL METHODS	34
5.1.1 BEAM THEORIES FOR FLEXURAL VIBRATIONS	34
5.1.2 WAVE PROPAGATION APPROACH	36
5.2 RESULTS AND DISCUSSIONS	36
5.2.1 ANALYTICAL VS FEM	36
5.2.2 WITHOUT DEFECTS	37
5.2.3 WAVINESS	40
5.2.4 PINHOLE DEFECT	41

5.2.5 VACANCY DEFECT	42
5.3 CONCLUSION	44
<b>CHAPTER 6 – NANOTUBE BASED MASS SENSORS</b>	<b>46</b>
6.1 ANALYTICAL METHODS	49
6.1.1 RESONANT FREQUENCIES WITH ATTACHED MASS	49
6.1.2 CANTILEVER CNT WITH MASS AT THE TIP	49
6.1.3 BRIDGED CNT WITH MASS AT THE MIDPOINT	50
6.2 RESULTS & DISCUSSIONS	51
6.2.1 ANALYTICAL VS FEM	51
6.2.2 WITHOUT DEFECTS	52
6.2.3 WAVINESS	54
6.2.4 VACANCY DEFECT	56
6.3 CONCLUSIONS	58
<b>CHAPTER 7 – CARBON NANOTUBE FRACTURE</b>	<b>59</b>
7.1 FRACTURE MECHANICS	60
7.1.1 STRESS INTENSITY FACTOR	61
7.1.2 J- INTEGRAL	62
7.2 RESULTS & DISCUSSIONS	64
7.3 CONCLUSIONS	66
<b>CHAPTER 8 - CONCLUSION &amp; FUTURE SCOPE</b>	<b>67</b>
8.1 CONCLUSIONS	68
8.2 FUTURE SCOPE	69
REFERENCES	70
LIST OF PUBLICATION	82

## LIST OF FIGURES

---

FIG NO	DESCRIPTION	PAGE NO
2.1	Vector diagram of carbon nanotube	6
2.2	Illustration of the three types of CNTs including a) zigzag, b) armchair and c) chiral	7
2.3	Transmission electron microscopy image of herringbone MWNT	8
2.4	Transmission electron microscopy image of a bamboo type MWNT	8
2.5	Arc discharge synthesis chamber	10
2.6	Laser ablation Setup	11
3.1	(9,0) CNT with Stone Wales defect	18
3.2	(5,5) CNT with Stone Wales defect	18
3.3	Waviness Factor, $w = A/H$ , associated with a typical nanotube [59]	19
3.4	Atomic geometry for vacancies. (a) one-vacancy in zigzag nanotube, (b two-vacancy in zigzag nanotube	21
3.5	Schematic views of a single pinhole defect of Type A with 6 atoms removed	21
3.6	Schematic views of a single pinhole defect of Type B with 24 atoms removed	21
3.7	Predicted fracture evolution in the (20,0) tube containing single atom vacancy defect	22
4.1	3-D Continuum model of CNT	29
4.2	Structural Mechanics model of CNT using beam elements	30
5.1	Nanomechanical oscillator based on doubly clamped CNT and gate electrode [104]	32



5.2	Frequency oscillations of MWNT core inside outer shell [106]	32
5.3	Use of molecular structural mechanics approach to study SWNTs as nanomechanical resonators [87]	33
5.4	Mode shapes for SWNT from molecular structural mechanics approach. Nanotubes are assumed to be rigidly clamped on both ends [87]	33
5.5	Comparison of analytical and FEM results for Fixed-free CNT	37
5.6	Comparison of analytical and FEM results for Fixed-fixed CNT	37
5.7	Different mode shapes for a fixed-free CNT	38
5.8	Effect of change of diameter on resonant frequency of fixed-free CNT	38
5.9	Effect of change of length on resonant frequency of fixed-free CNT	39
5.10	Effect of change of L/D ratio on resonant frequency of fixed-free CNT	39
5.11	Effect of chirality on the resonant frequency of fixed-fixed carbon nanotube	40
5.12	Effect of chirality on the resonant frequency of fixed-free carbon nanotube	40
5.13	Comparison between frequency of straight and wavy CNT for various length	41
5.14	Variation in frequency due to change in the waviness ( $e/L$ ) of CNT	41
5.15	Frequency ratio (Normalized frequency) for no. of defects for type A and Type B defect in CNT	42
5.16	Change in frequency with change in chiral angle with and without type A pinhole defect in CNT	42

5.17	Change in frequency as no of vacancy defect increases for fixed-free CNT	43
5.18	Change in frequency as vacancy defect moves towards free end in fixed-free CNT	43
5.19	Change in frequency as chirality increases CNT with no defect and with 4 defects	44
6.1	TEM photographs of a small particle attached at the end of a CNT nanocantilever vibrating at first harmonic resonance frequency [114]	47
6.2	Cantilevered and bridged nanotube resonator with an attached mass [89]	48
6.3	Cantilever SWCNT used as a atom mass sensor	48
6.4	Configuration of Carbon Nanotube resonator having waviness defined by ratio $e/L$ and mass attached at position 'a'	51
6.5	Comparison of analytical and FEM results for Fixed-free CNT	52
6.6	Comparison of analytical and FEM results for Fixed-fixed CNT	52
6.7	Effect of change of length on the frequency of fixed-free CNT	53
6.8	Effect of change of diameter on the frequency of fixed-free CNT	53
6.9	Change in frequency of mass sensors as mass at tip change in a fixed-free CNT	53
6.10	Effect of the change of position of mass along the length of a fixed-free CNT	54
6.11	Effect of the change of position of mass along the length of a fixed-fixed CNT	54
6.12	Effect of $a/L$ on the frequency for straight & wavy fixed-fixed CNT	55

6.13	Change in Frequency with increase in length of a fixed-fixed CNT	55
6.14	Change in Normalized frequency ( $F_{sav}/F$ ) of mass sensor for different masses for a fixed-free CNT	56
6.15	Effect of change in position of SAV in a fixed-free CNT	56
6.16	Change in frequency as the number of vacancy defects increases in a fixed-free CNT	57
6.17	Effect of chirality on the mass sensors with SAV defect in a fixed-free CNT	57
7.1	Independent Fracture Modes	62
7.2	J-Integral in two dimensions	63
7.3	J- Integral in three dimensions	63
7.4	Effect of CNT Length on the J and K1	64
7.5	Effect of CNT diameter on the J and K1	64
7.6	Effect of crack position on the J & K1 of CNT	65
7.7	Normalized J, $K_1$ and $K_2$ values for different chiral angle	65

## LIST OF TABLES

---

TABLE NO	DESCRIPTION	PAGE NO
4.1	Properties of CNT	28
4.2	Properties of Beam element	29

## NOMENCLATURE

---

<b>SYMBOLS</b>	<b>DESCRIPTION</b>
$C_h$	Chiral vector
$\alpha$	Chiral angle
$D$	Outer Diameter of CNT
$d$	Inner Diameter of CNT
$a_{cc}$	Carbon-carbon bond length
$w$	Waviness factor
$L$	Length of CNT
$I$	Moment of inertia
$E$	Young's modulus
$\rho$	Mass density
$A$	Cross-sectional area
$f_n$	$n$ th Mode Frequency
$\lambda_n$	Dimensionless parameter for $n$ th mode
$E_f$	Flexural modulus
$R$	Radius of curvature
$k$	Curvature parameter
$T_0$	Characteristic time constant
$\omega$	Non-dimensional frequency
$\Omega$	Frequency
$e$	Amplitude of waviness
$a$	Distance from fixed end
$t$	Time

$k_{eq}$	Equivalent stiffness
$m_{eq}$	Equivalent mass
$M$	Mass attached to CNT
$x$	Spatial coordinate
$Z$	Rise function
$K_I$ or $K_1$	Mode I stress intensity factor
$K_{II}$ or $K_2$	Mode II stress intensity factor
$K_{III}$ or $K_3$	Mode III stress intensity factor
$\sigma$	Stress
$K_{Ic}$	Fracture toughness
$J$	J integral
$W$	Elastic strain energy

**CHAPTER 1**  
**INTRODUCTION**

## **1.1 INTRODUCTION**

Carbon nanotubes are small cylinders of carbon atoms. They are not unlike other carbon materials such as diamond or the carbon black that can be found in pencils or car-tires. They have however a completely different structure that gives them interesting and very promising properties. Normal graphite is built of sheets with a honeycomb structure of carbon atoms. These sheets are very strong, stable and flexible, but adjoining sheets lack a strong cohesion. In nanotubes however these sheets are larger and are “rolled-up” to form long, thin spiral patterns. If this rolled-up sheet consists of one or more real tubes they are considered to be nanotubes. Carbon nanotubes (CNTs) are perhaps the most widely investigated nanomaterial because of their thermal [1], electrical [2], and mechanical [3, 4] properties. Discovered in 1991 [5], their promise of being a super material capable of endless applications is still primarily under research.

## **1.2 OBJECTIVE OF DISSERTATION**

The present work deals with the effect of defects on the mechanical properties of carbon nanotube (CNT) by finite element analysis. The work has been presented in the following sections by considering various aspects:

- Modelling and simulation of CNT using structural mechanics and continuum mechanics techniques.
- Comparing Analytical and FEM model.
- To study the effect of various defects of CNT on the properties of CNT.
- Effect of defects on change of length and diameter of CNT.
- Computing the effect of chirality on defective and non defective CNTs.
- Defects to be analysed are waviness, vacancy defect, pinhole defect and fracture.



### **1.3 OUTLINE OF DISSERTATION**

The work reported in this dissertation has been organized into eight chapters. The content in the chapters are briefly described below:

Chapter 1 gives an introduction to carbon nanotubes. This chapter also lists the objective of the present analysis along with outline of dissertation.

Chapter 2 deals with Carbon Nanotube structure, fabrication techniques, mechanical properties and application of CNT in various fields.

Chapter 3 gives details about modeling and simulation techniques used for carbon nanotube. This chapter is also deals with the modeling techniques, variables and assumptions used in present study.

Chapter 4 gives introduction to defects present in Carbon Nanotubes. All defects reported in research papers are detailed. Stone wals defects, waviness, pinhole defect and vacancy defects are described in this chapter.

Chapter 5 presents the study, results and discussion of CNT as nanomechanical sensors. This chapter deals with effects of various parameters like length, diameter, chirality, waviness, and other defects on the frequency of CNT.

Chapter 6 presents the study, results and discussion of CNT as mass sensors. This chapter deals with effects of various parameters like length, diameter, mass value, position of mass attached, chirality, and various other defects on the frequency of CNT.

Chapter 7 presents the study, results and discussion of CNT as structural member. This chapter deals with effects of various parameters like length, diameter, position of crack and chirality on the crack vulnerability of CNT.

Chapter 8 gives the conclusions of present work and the future scope of work.

**CHAPTER 2**

**CARBON NANOTUBES**

## **2.1 CNT STRUCTURE**

A CNT is comprised of one or many graphitic sheets, rolled up into a cylinder. Carbon can exist in many forms and take on varying chemical and physical properties. Carbon atoms have six total electrons, occupying the  $1s^2$ ,  $2s^2$ , and  $2p^2$  orbits. The bond strength between the valence electrons in the outer two orbits is weaker than that in the  $1s^2$  orbital, thus allowing a mixing or hybridization of the electrons. This mixing is made possible by the small energy difference between the  $2s$  and  $2p$  energy levels. The three possible hybridizations in carbon are  $sp$ ,  $sp^2$  and  $sp^3$  and three respective example materials include acetylene, polyacetylene, and methane. The physical characteristic that predominantly determines the behaviour of CNTs is the structure of the carbon atoms within the graphitic sheet. For example, the chirality of the CNT, the twist or wrap-angle of the nanotube with respect to its central axis, determines the electrical characteristics of the tube. The mechanical strength of CNTs, estimated higher than 1 TPa in the tensile direction, is also largely affected by the arrangement of the carbon atoms and the general defectiveness of this structuring. CNTs can be grouped into two classifications based upon the number of layers of graphitic carbon that comprise their sidewalls. Tubes consisting of one single layer are called single walled CNTs (SWNTs) and those having more than one layer of carbon are referred to as multiwall CNTs (MWNTs). CNTs of both types are of considerable interest depending upon the situation and applications.

### **2.1.1 SINGLE WALLED NANOTUBES**

Single walled nanotubes are viewed as the more promising type of nanotube for electrical applications due to their ability to be either conducting or semiconducting. The structure and conductivity of the nanotube is determined by the chirality of the nanotube, which is defined by its chiral vector, depicted as  $Ch$  in Fig 2.1 below.

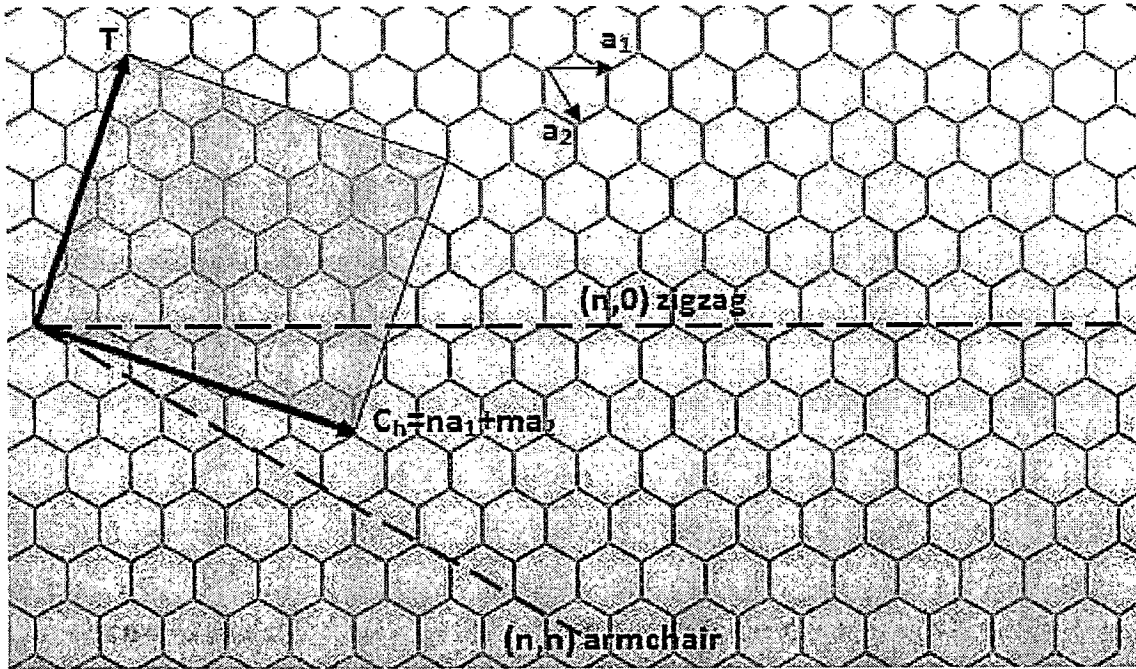
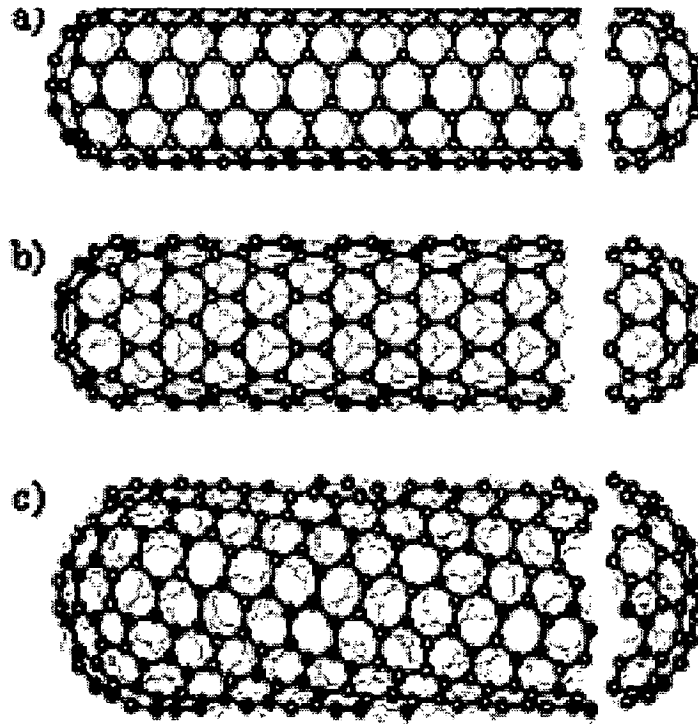


Fig 2.1: Vector diagram of carbon nanotube

The chiral vector defines the amount of twist present in the hexagonal network of carbon atoms with respect to the central axis of the tube. The formula for the chiral vector is

$$C_h = a_1 \cdot n + a_2 \cdot m$$

where  $n$  and  $m$  are integers and  $a_1$  and  $a_2$  are the basis unit vectors shown in the hexagonal carbon network above in Fig 2.1. The chiral angle  $\theta$ , defined by the angle between the chiral vector and one of the basis vectors, can never be greater than  $30^\circ$ . The chiral angle reaches a maximum of  $30^\circ$  when the nanotube basis vector integers are equal. The chiral vector is a minimum of  $0^\circ$  when the tube has coordinates  $(n,m)$  equal to  $(0,m)$  or  $(n,0)$ . The chiral vector dictates the geometric arrangement of the nanotube and there exist three distinct possible classifications. The names given for the three classes are armchair, in which  $n$  is equal to  $m$ ; zigzag, where  $m$  is equal to 0; and helical, in all other cases, are illustrated below in Fig 2.2.



**Fig 2.2:** Illustration of the three types of CNTs including a) zigzag, b) armchair and c) chiral

The approximate diameter of single walled nanotubes can be calculated from the  $n$  and  $m$  integers of the chiral vector,  $Ch$ . The nanotube diameter,  $D$ , can be given by,

$$D = \left| \frac{C_n}{\pi} \right| = \frac{a_{cc} \sqrt{3(n^2 + m^2 + nm)}}{\pi}$$

where  $a_{cc}$ ,  $1.41 \text{ \AA} \leq a_{cc} \leq 1.44 \text{ \AA}$ , is the average carbon-carbon bond length as found in graphite (lower limit) and in C60 fullerene molecule (upper limit)[6]. The smallest diameter nanotube that has been experimentally synthesized is  $4 \text{ \AA}$  [7]. The upper bound for SWNTs has not been experimentally determined, but calculations have shown that collapse due to van der Waals forces is favourable at diameters above  $25 \text{ \AA}$  [8]. Carbon nanotubes can be produced with very large aspect ratios, as SWNTs have been measured to lengths of several centimetres [9].

### 2.1.2 MULTIWALLED NANOTUBES

Multiwalled nanotubes (MWNTs) can be thought of as concentric single walled nanotubes of increasing diameter arranged in a nested, Russian doll type fashion. The material properties of MWNTs are mostly dependent upon the perfection and orientation of the graphitic planes comprising the MWNT [6]. Depending upon the structuring of the concentric nanotubes and the presence of slight imperfections, a multiwalled nanotube can exhibit a number of structural formations including herringbone and bamboo type. Herringbone MWNTs exhibit graphitic planes, also called graphene, at an angle to the central nanotube axis. When many such angled planes are stacked over a given length of the nanotube as seen in Fig 2.3, it looks similar to a herring backbone.

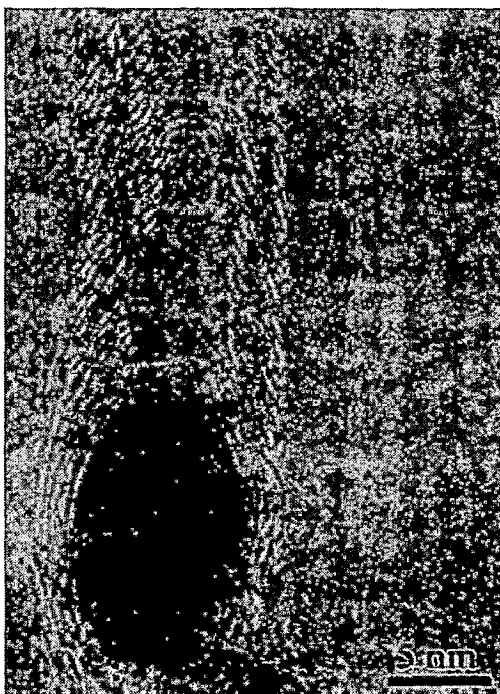


**Fig 2.3:** Transmission electron microscopy image of herringbone MWNT

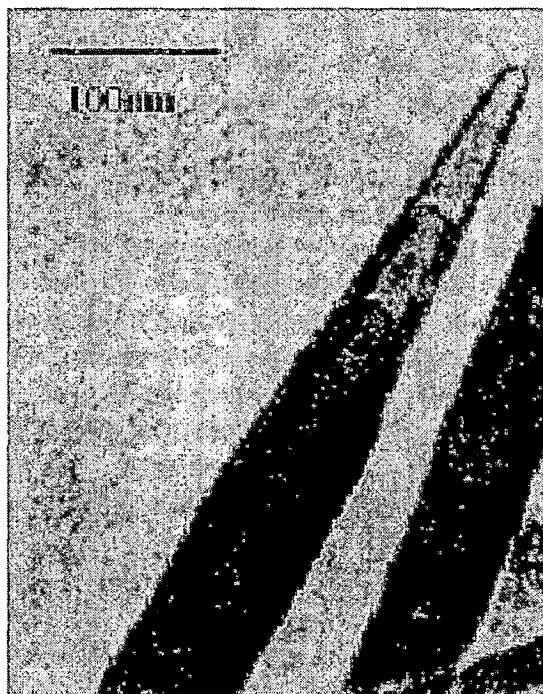


**Fig 2.4:** Transmission electron microscopy image of a bamboo type MWNT

Bamboo type MWNTs, shown in Fig 2.4 are characterized by the growth of graphene perpendicular to the central nanotube axis. This type of growth creates pockets within the nanotube similar to that of bamboo shoots.

## **2.2 CNT FABRICATION TECHNIQUES**

There exist many methods by which CNTs can be produced, including but not limited to chemical vapour deposition, arc discharge and laser ablation. Global synthesis attempts to produce CNTs in a high temperature environment directly on the actual microsystem, where the entire microsystem is exposed to the high temperature field. Synthesis methods such as arc-discharge [10, 11], laser ablation [12, 13], pyrolysis, and numerous types of chemical vapour deposition (CVD) [14-17] provide many different ways to produce CNTs. The synthesis of CNTs by the global CVD method is of great interest due to its ability to be easily modified and scaled-up in terms of quantities produced. The challenge of the CVD method lies in the multitude of parameters involved, any of which can have dramatic effects on the material produced [18]. The use of metal nanoparticles as a catalyst source to the CVD process is of great interest due to the large amount of commercially available particles and the low concentrations of particles in solution necessary to facilitate CNT growth. The use of nanoparticles and thin films as catalyst sources is a well documented method of providing catalyst to the synthesis reaction [19-22].

### **2.2.1 CHEMICAL VAPOUR DEPOSITION**

Chemical vapour deposition (CVD) is a synthesis technique that has existed for many years and is capable of depositing a number of materials. While the CVD method has been used since the 1960's to produce carbon filaments and fibers, it was not until the early 1990's that it was capable of producing CNTs. There are many types of CVD that can be used in the manufacture of CNTs, but the predominant types are thermal and plasma enhanced. Thermal chemical vapour deposition relies on thermal decomposition, or cracking, of carbonaceous gas molecules to introduce carbon into the vapour-liquid-solid (VLS) growth mechanism that subsequently forms CNTs. The VLS synthesis mechanism can be used in the synthesis of many types of one dimensional nanostructure and generally consists of the three primary

steps of absorption, saturation, and structure extrusion. A low melting point metal, with the ability to absorb the desired gas species, is typically used as a catalyst in the VLS mechanism. In the synthesis of carbon nanotubes, transition type metals such as iron, nickel, and molybdenum are used as catalyst for their ability to absorb carbon. The metal catalyst can be introduced via solution, evaporation or sputtering onto the synthesis substrate or into the synthesis chamber. The carbon source in t-CVD is most often carbonaceous gases including methane, acetylene and ethylene, but can also include vaporized carbon feedstock such as toluene.

### 2.2.2 ARC DISCHARGE

The arc discharge CNT synthesis method relies upon the vaporization of carbon in the presence of catalyst (iron, nickel, cobalt, molybdenum) while under a vacuum of inert gas such as argon or helium. The vital components inside of an electric arc chamber are the two graphite rods that provide the arc necessary for synthesis. After creating an arc between these two rods, plasma is formed consisting of a mixture of carbon vapour, catalyst vapour and the inert gas.

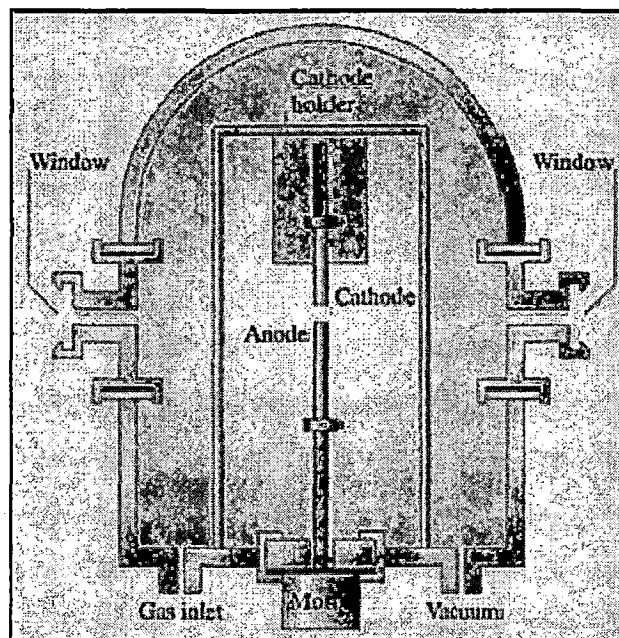


**Fig 2.5:** Arc discharge synthesis chamber



The two millimetre diameter rods are spaced a few millimetres apart, as shown in Fig 2.5 and typical arc power settings are an arc current of 80 amps and a generating voltage of 60 kilovolts. The catalyst is typically introduced into this reaction via the anode in two predominant methods, drilled hole or uniformly dispersed. By the drilling method, a several centimetre hole is drilled into the end of the anode graphite rod and filled with the catalyst and graphite powder. The other type of anode has the catalyst uniformly dispersed within the rod and is easier to fabricate.

### 2.2.3 LASER ABLATION

The CNT synthesis method of laser ablation is somewhat similar to arc discharge, in that both methods rely on the evaporation of solid graphite. While arc discharge relied upon a high voltage arc to create plasma, laser ablation utilizes a laser to add radiation energy to the synthesis reaction. Typically, a graphite pellet doped with a catalytic metal is placed inside the heated reaction zone of a furnace at around 1200 °C. A laser is then directed onto the pellet in a pulsed or steady fashion causing the vaporization of the metal and graphite. The metal is often slower to sublime than the graphite, causing the synthesis reaction rate to gradually slow over time as the pellet becomes more and more metallic. The heated vapours combine and are deposited onto a cooled copper surface as seen in Fig 2.6.

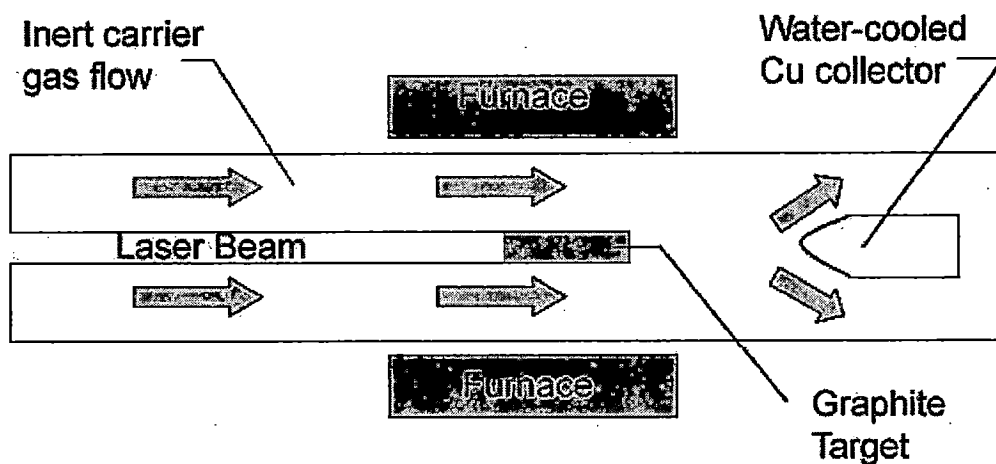


Fig 2.6: Laser ablation setup

The growth mechanism driving laser ablation and arc discharge are similar in character because both methods involve the vaporization of large carbon deposits and subsequent condensation. While the precise workings of the mechanism are not fully understood, it is known that the laser ablation and arc discharge growth mechanism is similar to the VLS mechanism of thermal CVD. One hypothesis of the growth mechanism, supported by experimental study, suggests that CNTs form during the cooling of stages of the synthesis process. At first the graphite target and catalyst particles are vaporized by either the laser or electrical arc, creating a very hot plume of vapour that quickly expands and cools. Large carbon clusters are formed as the vaporized carbon species begin to cool. As the catalyst cools, but more slowly at first, they begin to attach to the carbon clusters. Nanotubes form from these carbon-catalyst clusters until either the catalyst particle has become too large or until synthesis conditions have cooled and do not allow the carbon to diffuse in or onto the catalyst particles.

### **2.3 CNT MECHANICAL PROPERTIES**

CNTs have a number of enhanced material properties over their bulk counterpart of pure carbon. CNTs have strength to weight ratio higher than that of steel. The reason for the strength of CNTs in the axial direction is the sp<sup>2</sup> bonds within the graphite sheets. In previous experimental research, the Young's modulus of near perfect SWNTs in the axial direction has been estimated at 1 TPa [3]. In another study of CVD produced MWNTs the tensile strength was measured to be lower than 100 GPa. Reasons for differences between such estimates and measurements include point defects within the graphite planes and a misalignment of the graphitic planes with regard to the central axis. Nanoscale point defects should intuitively have a greater impact on nanotube sized features, versus their micro and macro sized fibres. Other more recent research, however has suggested that point and planar defects can act to strengthen MWNTs as they are strained in the axial direction [23]. There

are several methods available to measure the mechanical properties of CNTs, including bulk material analysis, resonance measurements, and Microsystems tooling measurements. Due to their high tensile strength and low density, CNTs have been viewed as an excellent choice for composite filling [24]. If sufficient knowledge of the alignment and volume fraction of the CNT filler is present, it is possible to back-solve for the average tensile strength of the CNTs. This method however, is not the best for obtaining mechanical property information from individual CNTs, due to uncertainties in the CNT dispersion and directional alignment. Another method for estimating mechanical properties of CNTs involves observing the amplitude of their thermal vibration and back solving for parameters using beam theory. This measurement is performed inside a scanning electron microscope (SEM) chamber while elevating the ambient temperature of the CNT sample. Although this measurement isolates individual CNTs, it requires the use of thermal vibration theory to extrapolate a material property. A third method of measuring the mechanical strength of CNTs is to use a micromanipulator tool such as an atomic force microscope probe. In this method, a CNT is mechanically attached to the sharpened tip at the end of a sensing MEMS cantilever. The other end of the CNT is then rigidly adhered to a surface using an epoxy or binder and a pulling, tensile force is then placed on the CNT. By noting the cantilever deflection and knowing the cantilever spring constant, it is possible to calculate the stress and strain being place on the CNT and hence make a calculation regarding its strength in the tensile direction.

## **2.4 APPLICATIONS OF CARBON NANOTUBES**

The special nature of carbon combines with the molecular perfection of single-wall CNTs to endow them with exceptional material properties, such as very high electrical and thermal conductivity, strength, stiffness, and toughness. No other element in the periodic table bonds to itself in an extended network with the strength of the carbon-carbon bond. The delocalized pi-electron donated by each atom is free to move about the entire structure, rather than remain

with its donor atom, giving rise to the first known molecule with metallic-type electrical conductivity. Furthermore, the high-frequency carbon-carbon bond vibrations provide an intrinsic thermal conductivity higher than even diamond.

In most materials, however, the actual observed material properties - strength, electrical conductivity, etc. are degraded very substantially by the occurrence of defects in their structure. For example, high-strength steel typically fails at only about 1% of its theoretical breaking strength. CNTs, however, achieve values very close to their theoretical limits because of their molecular perfection of structure. They open an incredible range of applications in materials science, electronics, chemical processing, energy management, and many other fields. Some of the applications related to mechanical field are discussed here.

#### **2.4.1 CARBON NANOTUBE COMPOSITES**

Incorporation of nanotubes into plastics can potentially provide structural materials with dramatically increased modulus and strength. The critical challenges lie in uniformly dispersing the nanotubes, achieving nanotube-matrix adhesion that provides effective stress transfer, and avoiding intratube sliding between concentric tubes within MWNTs and intrabundle sliding within SWNT ropes. Some promising results have been reported [25]. Researchers observed a monotonic increase of resistance to indentation by up to 3.5 times on loading up to 2% SWNTs and a doubling of thermal conductivity with 1% SWNTs. Also, 1% MWNT loading in polystyrene increases the modulus and breaking stress by up to 42 and 25%, respectively [26].

#### **2.4.2 SENSORS AND PROBES**

Possible chemical sensor applications of non-metallic nanotubes are interesting, because nanotube electronic transport and thermal power are very sensitive to substances that affect the amount of injected charge [27, 28]. The main advantages are the minute size of the

nanotube sensing element and the correspondingly small amount of material required for a response. Major challenges remain, however, in making devices that differentiate between absorbed species in complex mixtures and provide rapid forward and reverse responses. Carbon nanotube scanning probe tips for atomic probe microscopes are now commercially available. The mechanical robustness of the nanotubes and the low buckling force dramatically increase probe life and minimize sample damage during repeated hard crashes into substrates. The cylindrical shape and small tube diameter enable imaging in narrow, deep crevices and improve resolution in comparison to conventional nanoprobes, especially for high sample feature heights [28, 29]. Covalently modifying the nanotube tips such as by adding biologically responsive ligands, enables the mapping of chemical and biological functions [30]. Nanoscopic tweezers have been made that are driven by the electrostatic interaction between two nanotubes on a probe tip [31]. They may be used as nanoprobes for assembly.

**CHAPTER 3**

**DEFECTS IN NANOTUBE**

CNTs have superior properties compared to the traditional engineering materials. However, these properties hold only for the ideal case of carbon nanotubes where they are made of perfect hexagonal graphite honeycomb lattice of mono-atomic layer thickness. Each main advance in SWNT synthesis [13, 32–35] reasserts the claim of defect-free materials, usually supported by macroscopic characterization such as Raman spectroscopy [36–38]. Such claims are difficult to substantiate at the extremely low defect densities that affect device electronics, in part because of the experimental difficulty of directly imaging point defects. Atomic-resolution scanning tunnelling microscopy (STM) is a powerful technique for identifying SWNT defects [39–41]. Raman spectroscopy lacks the resolution to directly identify a single defect in otherwise pristine material [42]. As a result, current attempts to commercialize nanotube-based electronics such as logic, memory and chemical sensor circuits are proceeding with little quantitative knowledge about the defect sites in SWNTs, even though such sites may disproportionately affect the chemical, mechanical and electronic properties of SWNTs and critically enable or disable desirable properties [43]. An electrochemical method is used that labels point defects and makes them easily visible for quantitative analysis [44].

In general, the advantages or disadvantages of the presence of defects in carbon nanotubes depend on their applications. For example, structural defects may increase the adhesion of other atoms and molecules to carbon nanotubes [46]. The possibility of connecting two nanotubes with different chiralities by introducing heptagon and pentagon in the perfect hexagonal graphite lattice is addressed by Dunlap [45]. The application of CNTs in hydrogen storage systems has been under investigation in recent years [46]. It is suggested that the hydrogen uptake may be dominated by interactions with open-shell edges or defect sites in the nanotube structure. Zhu et al. [46] proposed that introducing defects on side walls of the CNT could be a potential technique to efficiently enhance the hydrogen uptake capacity of

such system. However, defects in the CNTs structure may alter their properties, in turn warranting detailed analyses of the effects of defects in carbon nanotubes: Studies show that even individual vacancies in CNTs change fracture behaviour [47].

### 3.1 STONE WALS DEFECTS

The most common topological defect “Stone-wales” defect is a combination of two pentagons and two heptagons (5-7-7-5 defect). This kind of defect causes little change to the diameter and chirality and the deformation effect is rather local. This transformation effectively elongates the tube in the strain direction, releasing the excess strain energy. This defect is can be incorporated in a normal tube by 90° rotation of carbon – carbon bond between two hexagons. This rotation changes four neighbouring hexagons into two pentagons and two heptagons as shown in Fig 3.1 & 3.2 [48].

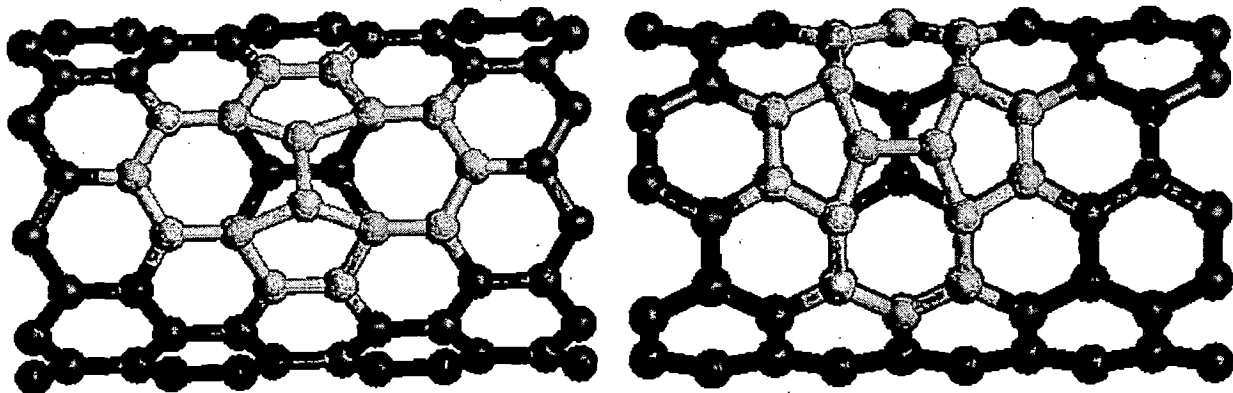


**Fig 3.1:** (9, 0) CNT with Stone Wales defect    **Fig 3.2:** (5, 5) CNT with Stone Wales defect.

Such bond rotation defect was observed to determine the size of the band gap. For example the defects introduced in a semiconductor nanotube make the tube metallic in character by closing the band gap. The same defect in metalized CNT show much stronger one-dimensional effects than the defect-free metallic nanotube [49, 50].



### 3.2 WAVINESS IN THE CNT

In most of the models and simulation of CNT dynamics, the nanotube was assumed to be perfectly straight. However, photomicrographs of nano-composites indicate that the nanotubes may exhibit significant waviness. Qian et al. [26] showed waviness in CNT in images taken by the transmission electron microscope. The effects of waviness have been proved to be significant on the elastic modulus of CNT. Fisher et al. [51,52] implemented a 3D finite element models for CNT- reinforced polymer composites. Gibson and Anumandle [53] developed a closed form micromechanical model for predicting the elastic modulus of a wavy CNT-reinforced polymer composite. Comparing the predictions of this model with experimental results for a MWNT reinforced polystyrene composites [54] showed that the model significantly over predicts the composite modulus unless significant waviness is assumed Berhan and Sastry [55] analyzed analytically the effect of waviness on the modulus of elasticity of CNT. The study is based on images taken by the scanning electron microscopes, which showed both straight and sinusoids segments of CNT. In the study by Fisher and Bradshaw [56], a 3D finite element model for an infinitely long wavy nanotube embedded in a matrix showed the impact of the waviness on the effective reinforcing modulus. They suggested that increasing the waviness in nanotube reduce the elastic modulus of it.

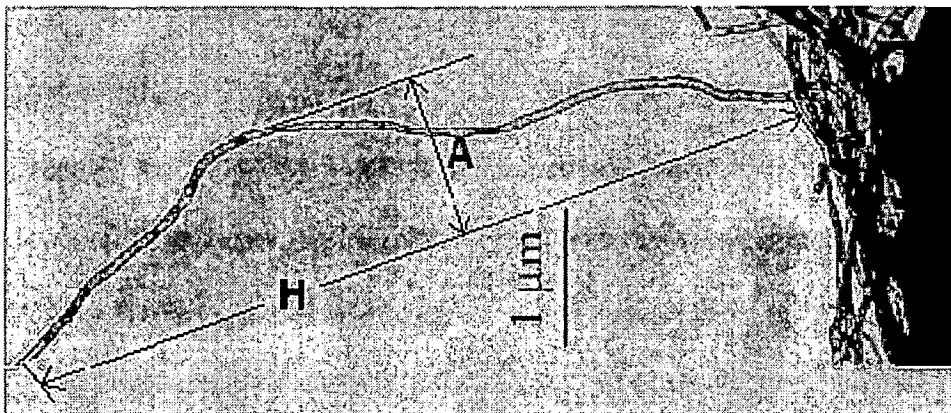
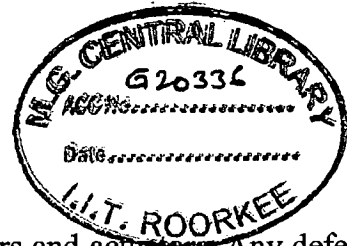


Fig 3.3: Waviness Factor,  $w = A/H$ , associated with a typical nanotube [59].

According to their statistics, the waviness is most likely to be in the range from 0.05 to 0.5. Wang and Poncharal [57] used the technique of TEM - transmission electron microscopy to capture the vibrations of the carbon nanotube. They did not study the effect of waviness or curvature of the CNT on the vibration behaviour; however their images showed clearly the existing of the curved nanotube which vibrates as a curved member. This is also supported by the experiments from Gao and Wang [58]. The wave propagation approach was proposed by Kang, et al. [60]. The wave propagation approach can be used for the free vibration analysis of a planar circular curved beam.

### 3.3 VACANCY DEFECT



Carbon nanotubes are widely used in the design of nanosensors and actuators. Any defect in the manufactured nanotube plays an important role in the natural frequencies of these structures. The carbon nanotubes act as basic elements of these nanostructures; therefore vibrations of CNTs get considerable importance. But most of the researches have focused on the simulation and estimation of the mechanical properties of perfect CNTs and have ignored the effect of initial defects. Whereas experimental observations have reported the presence of topological defects, such as the Stone Wales (SW) defect and vacancy defects (Fig 3.4) in CNTs [61]. Tserpes and Papanikos studied the effect of SW defect on the tensile behavior and fracture of armchair, zigzag and chiral SWCNTs [62]. In contrast to zigzag SWCNTs, their results show a significant reduction in the failure stress and the failure strain for armchair ones, ranging from 18% to 25% and from 30% to 41%, respectively. The results of chiral SWCNTs were reported between the results of zigzag and armchair ones. Mielke et al. used quantum mechanical calculations to explore the role of vacancy defects on the fracture of CNTs under axial tension [47]. Their results expose a reduction in the failure stress about 26%. Chandra et al. studied the SW defect in CNTs [63]. They have reported reduction of the

stiffness at the defected area by 30–50%. The effect of vacancy defects on the vibration of carbon nanotubes is investigated by using molecular structural mechanics method [64].

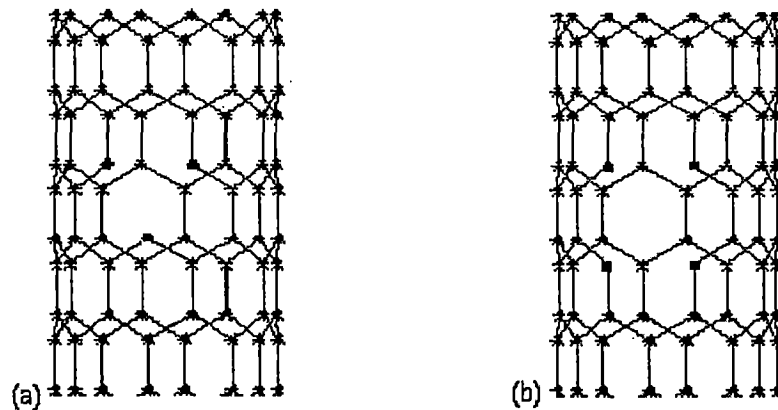


**Fig 3.4:** Atomic geometry for vacancies. (a) one-vacancy in zigzag nanotube, (b) two-vacancy in zigzag nanotube

### 3.4 PINHOLE DEFECT

Various defects on the CNT wall have been reported, which are formed during the synthesizing process. Some of them are reported to be large sufficiently for  $C_{60}$  molecule or metal molecules to pass through. In applying the CNT to nano-probes or nano-cantilever beams, the defects would affect the mechanical characteristics such as yield strength and a resonant frequency.

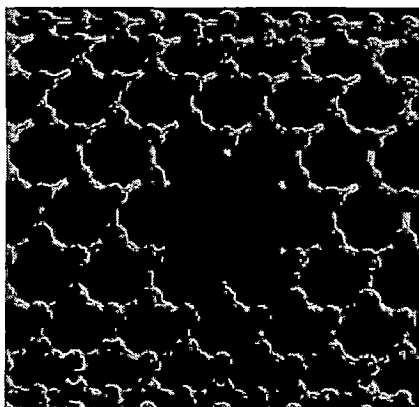


**Fig 3.5:** Schematic views of a single pinhole defect of Type A with 6 atoms removed

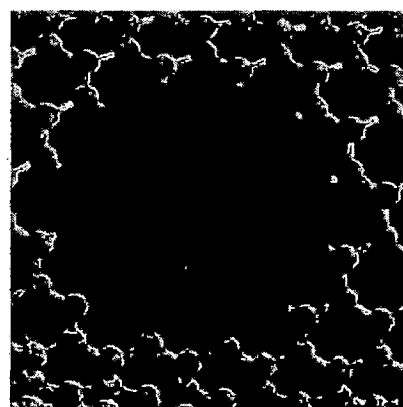


**Fig 3.6:** Schematic views of a single pinhole defect of Type B with 24 atoms removed

Few papers [65] are available regarding pinhole defect in CNT. In this report CNT with artificial pinhole defects are studied based on a continuum mechanics and atomic structure model. Simulation results are used to investigate the influences on vibration properties for various types of the CNTs and the number of the defects. In literature two kind of artificial pinhole defects are proposed as shown in Fig 3.5 & 3.6.

### 3.5 FRACTURES IN CNT

The effective use of CNTs in structural applications depends on their mechanical performance as standalone units. Mechanical properties and deformation of CNTs have been extensively studied during the last few years both experimentally and theoretically.

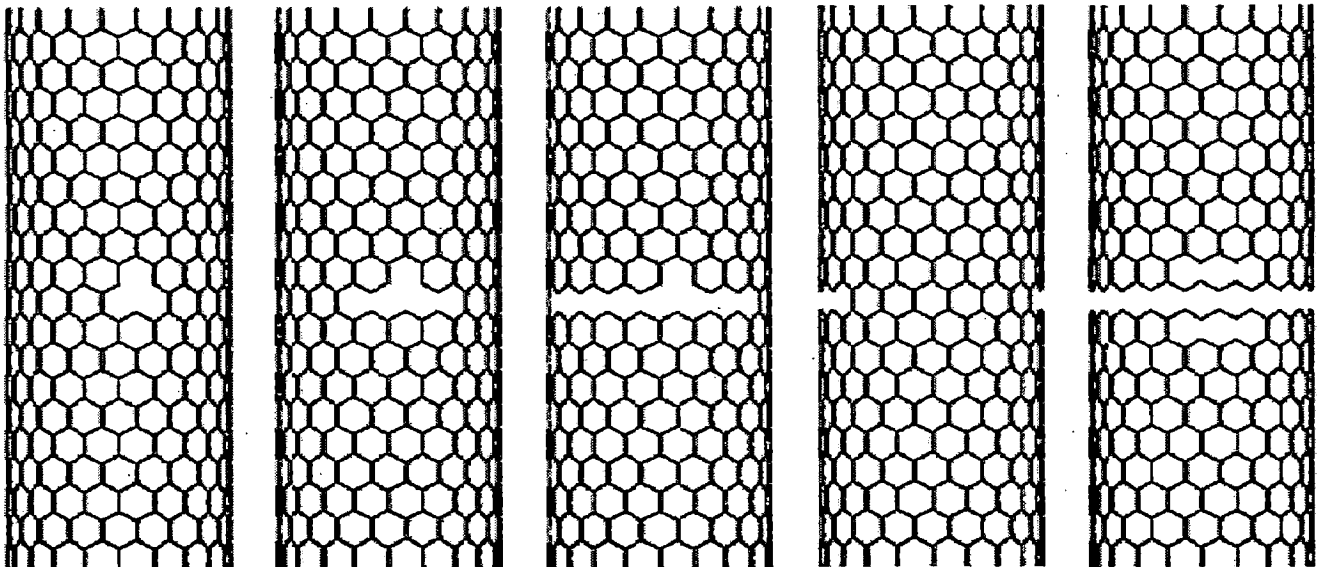


**Fig 3.7:** Predicted fracture evolution in the (20,0) tube containing single atom vacancy defect.

From the viewpoint of theoretical modelling, two approaches have been mainly adopted: the atomistic approaches (classical molecular dynamics (MD) and mechanics (MM)) and the continuum mechanics approaches. In the majority of studies, CNTs have been simulated as defect-free materials neglecting both the effect of initial defects as well as the effect of any possible fractures that might appear during loading. The only studies that have considered such effect, and therefore, are able to give information about the mechanical performance of

CNTs, are the MM and MD simulations of Belytschko et al. [66], Mielke et al. [67], Liew et al. [63] as well as the measures of stress and strain at the atomic scale of Chandra et al. [67]. Belytschko et al. [64] have studied fracture of CNTs under axial tension by MM simulations as shown in Fig 3.7. They found that the fracture behaviour is almost independent of the separation energy and dependant on the inflection point of the interatomic potential. The failure strain of a zigzag nanotube was predicted to be between 10 and 15%, which compares reasonably well with experimental results. Contrary to failure strain, the failure stresses were found to be 65–93 GPa, which are markedly higher than the experimental ones. Mielke et al. [47] used quantum mechanics calculations using density functional theory and semiempirical methods and MM calculations with a Tersoff–Brenner potential to explore the role of vacancy defects in the fracture of CNTs under axial tension. These methods showed reasonable agreement with experiments, although the MM scheme systematically underestimated the fracture strengths. Liew et al. [67] used MD simulations, performed in the microcanonical ensemble, to simulate the plastic deformation due to formation of Stone–Wales defects and the brittle fracture due to bond breaking. Chandra et al. [63] adapted three stress measures at atomic scales and introduced strain measures as energetically conjugate quantities to study the mechanics of Stone–Wales defect in various single-walled CNTs. It is found that the stiffness of the defected area is reduced by about 30–50% resulting in reduction of the nanotube Young’s modulus. The only continuum mechanics approaches that have modelled the exact atomic lattice of CNTs are the structural mechanics approach of Li and Chou [68] and the FE model of Tserpes and Papanikos [69], which is the base for the current work. The atomistic simulations are limited in both time and length scales. For example, a 10 nm long single-walled CNT (SWCNT) involves more than 2000 atoms and its atomistic study is computationally intensive.

**CHAPTER 4**

**MODELLING AND SIMULATION**

## **4.1 MODELLING & SIMULATION TECHNIQUES**

With the emerging field of nanotechnology, there seems a greater need than ever to be able to carry out computational simulations. This is because the material and devices related to the nanotechnology are often on the atomic scale and thus extremely difficult and costly to fabricate & manipulate. With the increasing computational power over the past few years and improvements in theoretical method and algorithm and finite element techniques, the capability of simulation has greatly expanded. Some of these techniques are described below:

### **4.1.1 MOLECULAR DYNAMICS**

In MD simulations, each of the CNT atoms is assigned with a potential and its equation of motion is evaluated at every time step. Several types of potentials were used, the most common being a bond order potential developed by Tersoff and Brenner [70], which was extended in [71], but also the molecular mechanics force field: MM3 [72] was used. As MD retains the atomic details of the molecule, it enables to simulate the effect of the chirality of CNTs and also the interactions between CNTs with other materials (such as proteins, hydrogen [73] and other atoms) at the atomic level. MD also facilitates simulations concerning nano- scale effects, such as radial deformation caused by vdW forces [74], CNT buckling [75, 76], nanotube self-healing [77, 78], closed ring structures [79], nanotube growth [80], and tube-substrate interactions [81]. Another goal of MD simulations is to obtain the macroscopic properties of CNTs in order to create continuum models. This was done by “virtual tests” of axial compression [82] or lateral, axial [83] and torsional deformations [84]. The continuum parameters are particularly desired because if the tube behaves in a continuum mechanical manner, simple analytical relations can be used to describe its mechanics. MD was also used to study small NEMS structures, such as switches [85, 86]. Due to the atomic nature of MD, large scale simulations are computationally demanding, thus, realistic NEMS are currently not simulated with MD.

### **4.1.2 STRUCTURAL MECHANICS**

An additional atomistic model is the SM approach [69]. In this model the bonds between every two nearest-neighboring atoms act like load-bearing beams and each atom acts as the joint of the related beams. This method was used to predict the fundamental frequencies of SWCNT and MWCNT mechanical resonators [87, 88]. SM was used to study the frequency shift in cantilevered and bridged SWCNT resonators induced by a mass change due to an attached particle [89]. SM was also used to estimate the Q-factor of CNT resonators as a function of temperature [90]. The findings of SM simulations are in good agreement with the existing theoretical and experimental results.

### **4.1.3 DISSIPATIVE PARTICLE DYNAMICS**

In atomistic methods the number of particles in the simulation is equal to the number of atoms in the real systems, hence as the scale of the system under consideration grows, the complexity of the simulated system becomes computationally challenging. Coarse grained methods (e.g. DPD [91]) offer an attractive solution and allow computationally efficient mesoscale simulations. Using DPD, it is possible to retain the particle based structure of the system, while the number of particles in the simulation is reduced. An additional major advantage of DPD is the feasibility to seamlessly couple different length scales. Thus, simulations of multi-scale systems, such as CNTs on various substrates, interaction of CNTs with gas molecules and the interaction of CNTs with one another can be easily and efficiently implemented. The dispersion of CNTs into a polymer matrix was modelled successfully using DPD and Flory-Huggins theory [92]. The CNTs in [92] were modelled as simple chains with certain rigidity while discarding the tubular structure of the CNTs.



#### **4.1.4 CONTINUUM MECHANICS**

In spite of the constant increase in the last several years in computational speed, storage availability and improvement in numerical algorithms, MD computations are still limited to simulations on the order of  $10^6$  atoms for only a few nanoseconds [93]. The simulation of larger systems or longer times can only be achieved by other methods, typically, continuum methods. In continuum methods, however, mechanical simulation methods completely discard variations over lengths on the order of the atomic scale as well as the atomic structure of the CNTs. Several advanced methods were developed toward continuum simulations and were applied to CNTs. Some of these methods are reviewed in [93] and include the quasi-continuum method [94-96], which incorporates interatomic interactions into an adaptively refined finite elements model through a crystal calculation, and the equivalent-continuum model [97], in which a representative volume element of the chemical structure of graphene was substituted with equivalent-truss and equivalent-continuum models. The basic continuum shell model was also shown to describe the mechanics of CNT accurately when the proper parameters are chosen [82]. Finite elements (FE) analysis packages, such as ABAQUS were implemented to produce results which are very similar to experimental observations, such as the rippling of nanotubes at large deformations [98].

#### **4.1.5 OTHER SIMULATION METHODS**

A mesoscale simulation is described in [99], which is based on a coarse grained representation of CNTs as breathing flexible cylinders consisting of a variable number of segments. The mesoscopic model has shown to reproduce well the dynamical behaviour of individual CNTs predicted in atomistic simulations at a fraction of the computational cost. Multiscale simulations couple several simulation methods which model different scales into one simulation. Multiscale methods have the benefit of atomistic detail localized in regions where it is necessary where quantities vary quickly on the atomic length scale, along with the

computational efficiency of less detail where small scale variations are unimportant or can be sufficiently regarded within the average quantity. An example of a multiscale simulation is a simulation of a resonant oscillator [100] which is based on an MD model for the CNT and a CM model for the paddle. The merging of different regions described by different scales has to be done carefully [101]. Additional multiscale methods are reviewed in [93]. Non dynamic simulation techniques were also used to obtain the mechanical properties of CNTs. Some of these methods are the empirical force constant model [102], tight binding, electronic band theory and quantum mechanical methods such as Density-functional theory and Hartree-Fock [83]. These simulation methods can be used to measure the elastic properties of CNTs; however they are not dynamic mechanical simulations.

## 4.2 MODELLING AND SIMULATION PARAMETERS

Two types of modelling techniques are used in this work – Continuum Mechanics and Structural Mechanics technique. All the parameters taken in to account are described below.

### 4.2.1 CONTINUUM MECHANICS

In this technique a 3-D solid model of the carbon nanotube is made. Material is assumed to be isotropic with the following properties

**Table 4.1:** Properties of CNT

Elasticity	1.1 TPa
Density	1330 Kg/m <sup>3</sup>

In this modelling technique thickness of the carbon nanotube is assumed to be 0.34 nm. Length and the diameter can be varied based on the requirement. Continuum model of a CNT with diameter of 1.1nm and length of 20nm is shown in Fig 4.1. In continuum mechanics model chirality can't be accounted. In this work continuum mechanics technique is used for modelling faultless CNTs, pinhole defect, waviness and crack in CNT.

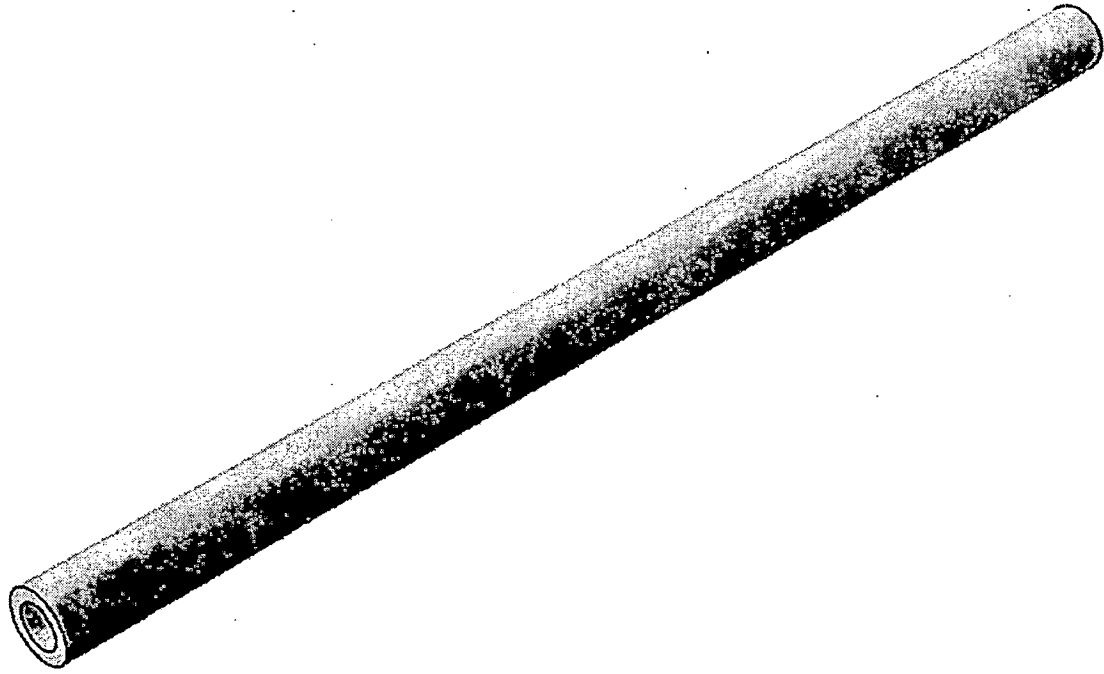


**Fig 4.1:** 3-D Continuum model of CNT

#### **4.2.2 STRUCTURAL MECHANICS**

In this technique the carbon nanotube bonds are treated as beam element and weight of carbon atom ( $1.99E-26$  Kg) is applied to each bond junction. The beam properties used are described in Table 4.2. Fig 4.2 shows a structural mechanics model of (5,5) CNT with length of 50 nm. Different type of chiral CNTs can be modelled using structural mechanics approach. In present report effect of chirality and vacancy defects are modelled using this approach.

**Table 4.2:** Properties of Beam element

Cross section Diameter	0.147 nm
Modulus of Elasticity	5.49 TPa
Shear Modulus	0.871 TPa

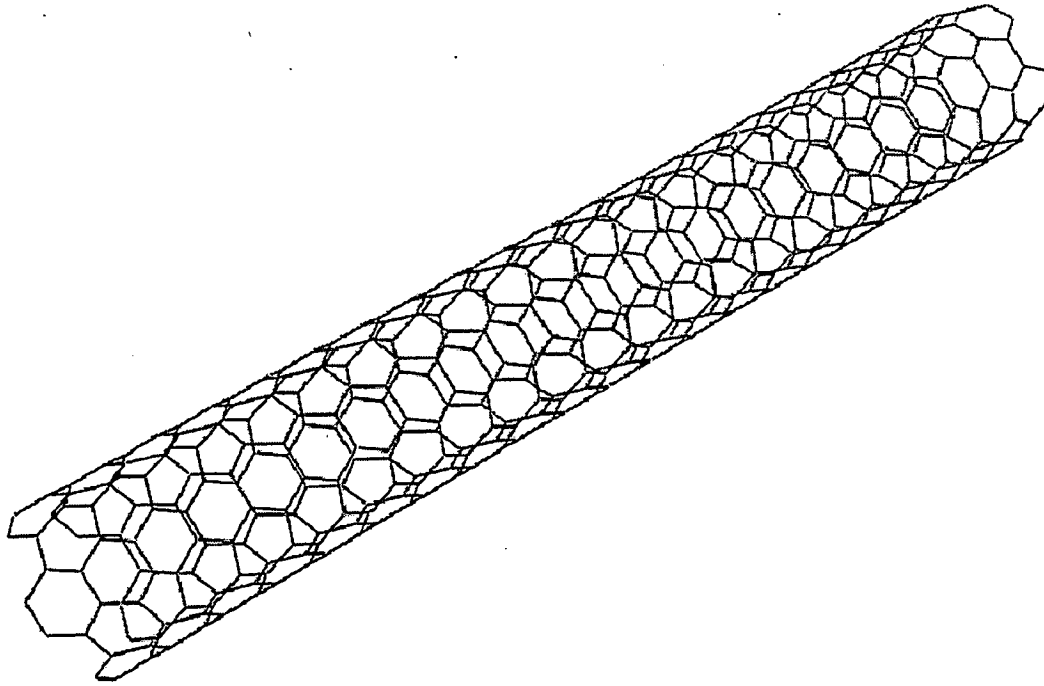


**Fig 4.2:** Structural Mechanics model of CNT using beam elements.

## **CHAPTER 5**

# **NANOMECHANICAL RESONATORS**

Nanometer-scale high frequency resonators are critical components of many nanoelectromechanical systems (NEMS) such as oscillators, charge detection devices, parametric amplifiers, nanoscale clocks and resonant sensors [103–105]. For example, Sazanova et al. [104] have developed a nanoelectromechanical oscillator based on the electrostatic actuation and detection of a double-clamped CNT with a gate electrode, as shown in Fig 5.1.

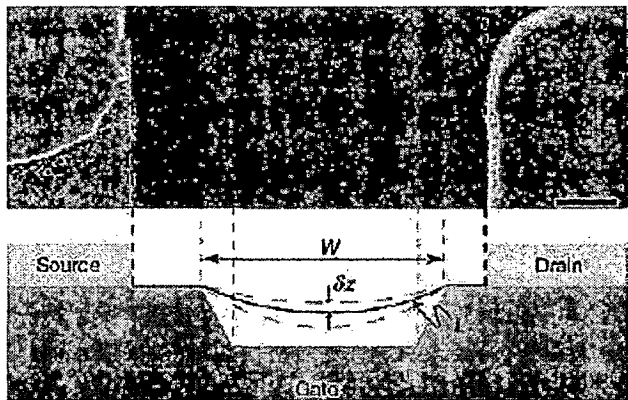


**Fig 5.1:** Nanomechanical oscillator based on doubly clamped CNT & gate electrode [104].

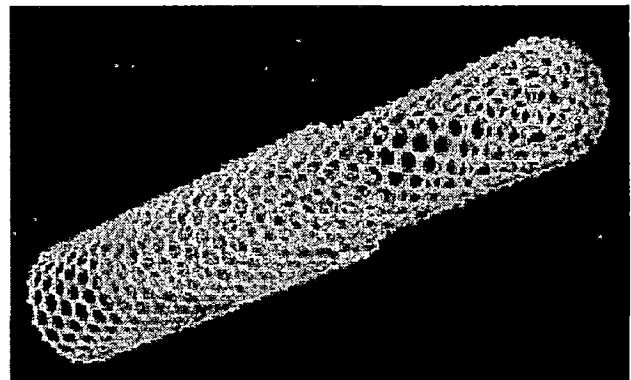


**Fig 5.2:** Frequency oscillations of MWNT core inside outer shell [106].

Zheng et al. [106,107] have proposed the design of an oscillator which should have an operating frequency of several Gigahertz based on the oscillation of the inner tube of a MWNT with respect to the outer tube of the MWNT. As shown in Fig 5.2, the inner tube, or core, is assumed to oscillate inside the outer tube about the position of minimum van der Waals potential energy. Liu et al. [108] used molecular dynamics simulations of MWNTs to show that the oscillatory frequencies saturate as the number of outer tubes exceeds three. Schwab [109] has shown that by fabricating a single-electron transistor onto a mechanical system in a high magnetic field, the mechanical spring constant and the damping constant of a CNT nanomechanical resonator can be manipulated by adjusting the potential of a nearby gate electrode. A molecular structural mechanics approach [68] has been used to predict the fundamental frequencies of cantilevered or bridged single wall carbon nanotube (SWNT)

nanomechanical resonators shown in Fig 5.3 indicate that these frequencies could reach the level of 10 GHz–1.5 THz [87].

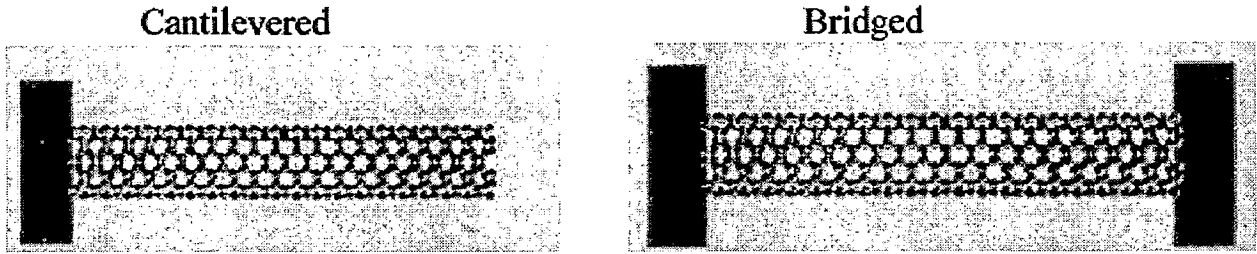


**Fig 5.3:** Use of molecular structural mechanics approach to study SWNTs as nanomechanical resonators [87].

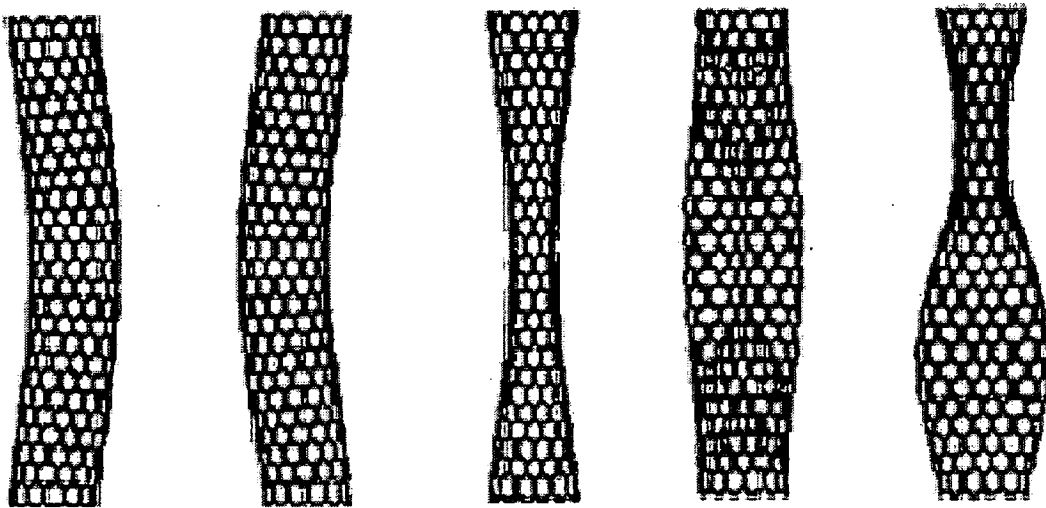


**Fig 5.4:** Mode shapes for SWNT from molecular structural mechanics approach. Nanotubes are assumed to be rigidly clamped on both ends [87].

Typical predicted mode shapes were shown previously in Fig 5.4. It has been reported that ropes consisting of hundreds of SWNTs have flexural frequencies in the MHz range [110]. Individual cantilevered SWNTs having aspect ratios (i.e., ratio of length  $L$ -to-outside diameter  $D$ ) of approximately  $L/D = 100$  were also found to have fundamental flexural resonance frequencies in the MHz range [53]. Resonator or oscillator arrays based on CNTs have been shown to be effective nanoelectromechanical signal processing devices for transmission of RF signals [111]. The nanotube array, which is based on vertical CNT arrays integrated with waveguides and bias electrodes, serves to transmit the RF signal only at its

mechanical resonance frequency and reflects RF power at all frequencies except the mechanical resonance frequency. At the CNT array resonance frequency, the incident RF wave couples to nanotubes near the input electrode due to Coulomb forces between the RF electric field and the electric charge on the CNTs. In related work, it has been proposed that a CNT film grown on a quartz surface could be used as a miniaturized RF filter [112].

## 5.1 ANALYTICAL METHODS

### 5.1.1 BEAM THEORIES FOR FLEXURAL VIBRATIONS

Beam theories for flexural vibrations fall into the category of continuum modelling approaches. These theories can be used to estimate the theoretical fundamental flexural resonance frequencies of CNTs. In many experimental studies, classical beam theories have been used to “back out” the modulus from the measured resonance frequencies of cantilevered CNTs. If nanotubes are to be used as nanomechanical resonators, it is important to have accurate theoretical models for prediction of the natural frequencies and mode shapes. According to Bernoulli-Euler theory, the flexural motion of a homogeneous, isotropic, linear elastic straight beam without shear or rotary inertia effect is described by the following equation

$$-\frac{\partial^2}{\partial x^2} \left( EI \frac{\partial^2 w}{\partial x^2} \right) = \rho A \frac{\partial^2 w}{\partial t^2}$$

where

$I$  = moment of inertia of cross section about its neutral axis

$E$  = effective Young’s modulus of the beam material

$\rho$  = effective mass density of beam material

$A$  = cross-sectional area of the beam

$w(x,t)$  = transverse displacement of the centroidal axis of beam

$x$  = distance along beam

$t$  = time



In case of a CNT, E and I values are constant along the length, therefore equation will reduce to

$$EI \frac{\partial^4 w}{\partial x^4} + \rho A \frac{\partial^2 w}{\partial t^2} = 0$$

The corresponding frequency equation for flexural vibration is

$$f_n = \frac{\lambda_n^2}{2\pi L^2} \sqrt{\frac{EI}{\rho A}}$$

where

$f_n$  - nth mode frequency, Hz

L – length of beam

n – mode number

$\lambda_n$ - dimensionless parameter for nth mode

The dimensionless parameter  $\lambda_n$  is a function of the boundary conditions applied to the beam.

First three dimensionless parameters for fixed-free cantilever beam are  $\lambda_1 = 1.87510407$ ;  $\lambda_2 = 4.69409113$ ,  $\lambda_3 = 7.85475744$  and the corresponding values for the fixed-fixed conditions are  $\lambda_1 = 4.73004074$ ,  $\lambda_2 = 7.85320462$ ,  $\lambda_3 = 10.9956079$ . For a SWCNT or any beam having tubular geometry with outside diameter  $D_o$  and inside diameter  $D_i$ , the above equation becomes

$$f_n = \frac{\lambda_n^2}{8\pi L^2} \sqrt{\frac{(D_o^2 + D_i^2)E}{\rho}}$$

If the beam bends by elongation of the outer arc and a compression of the inner arc of the bend as in the case of CNTs, then E will be replaced by flexural modulus,  $E_f$ . Also if the properties of the beam vary through the thickness of the beam, E in the above equation should be replaced by  $E_f$ .

## 5.1.2 WAVE PROPAGATION APPROACH

All of the equations in the previous section are based on the assumption that the beam is straight. But it shown that CNT inherent waviness. So wave propagation approach can be used to get the theoretical natural frequencies at various waviness factors

$$k^2 = \frac{I}{AR^2}$$

$$T_0 = R^2 \sqrt{\frac{\rho A}{EI}}$$

$$\Omega = \frac{\omega}{T_0}$$

where I - second moment of inertia of the cross-section about the centroid

R - constant radius of curvature for given range of angles

A - cross-sectional area

k - curvature parameter

$\rho$  - mass density

E - Young's modulus

$T_0$  - characteristic time constant

$\omega$  - non-dimensional frequency

$\Omega$  - frequency in rad/sec

The values of all the parameters mentioned above can be calculated at various waviness factors [60, 114].

## 5.2 RESULTS AND DISCUSSIONS

### 5.2.1 ANALYTICAL VS FEM

Analytical as well as FEM results are computed for both cantilever and bridged CNT. Fig 5.5 shows that FEM and analytical results are approximately same and vary by maximum of 2.5 %. Frequency variation is computed for length of 20nm to 60nm and CNT with diameter of 1.1nm. Fig 5.6 Shows the same results but for a bridged CNT. Length of the CNT is varied from 20nm to 60nm and diameter is taken as 1.1nm. Results between analytical and FEM are found to be varied by approximately maximum of 5%.

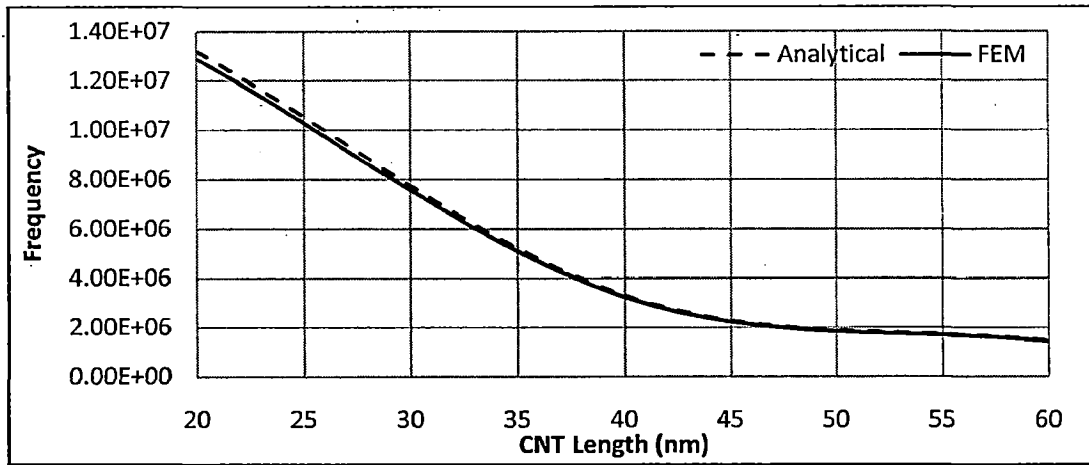


**Fig 5.5:** Comparison of analytical and FEM results for Fixed-free CNT

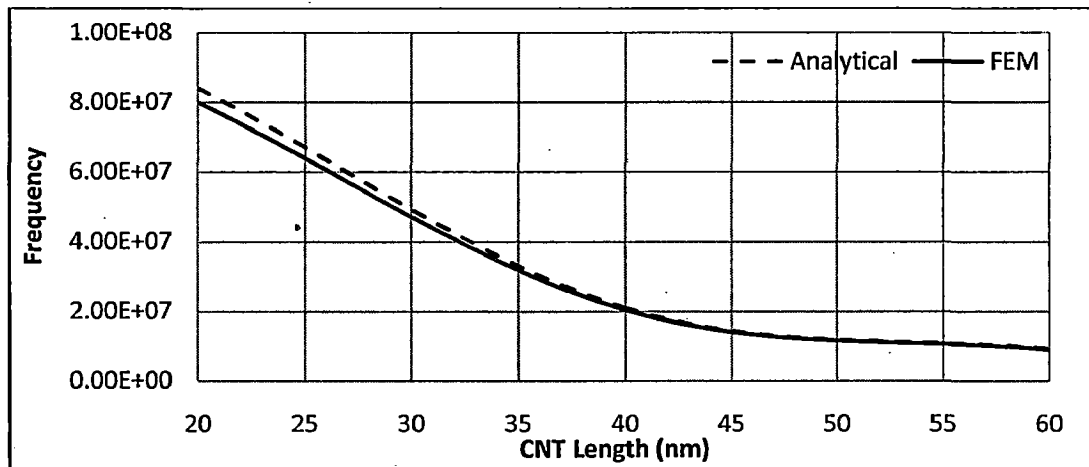


**Fig 5.6:** Comparison of analytical and FEM results for Fixed-fixed CNT

### 5.2.2 WITHOUT DEFECTS

Resonant frequency for carbon nanotube is taken for different combinations of CNT structures for with or without various defects. Fig 5.7 shows the CNT and its different modes computed using ABAQUS. Fig 5.8 shows that as the diameter of the CNT increases the frequency of the CNT also increases. Length of the CNT is kept constant at 30nm. Results show that the change in frequency is linear for diameter values selected. Fig 5.9 shows that as the length of the CNT increases frequency decreases. For this analysis CNT diameter is taken as 2nm. Change in frequency is not linear for length change as they were observed for diameter change.



**Fig 5.7:** Different mode shapes for a fixed-free CNT

Most of the previous research results are based on L/D ratio so Fig 5.10 predicts that as the L/D ratio increases the frequency of CNT decreases which is in agreement with previous results predicted.

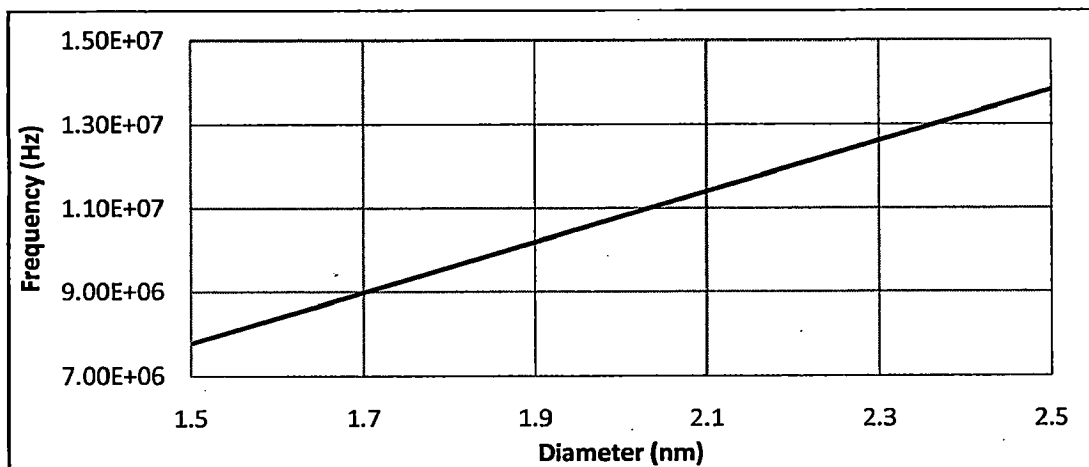


**Fig 5.8:** Effect of change of diameter on resonant frequency of fixed-free CNT

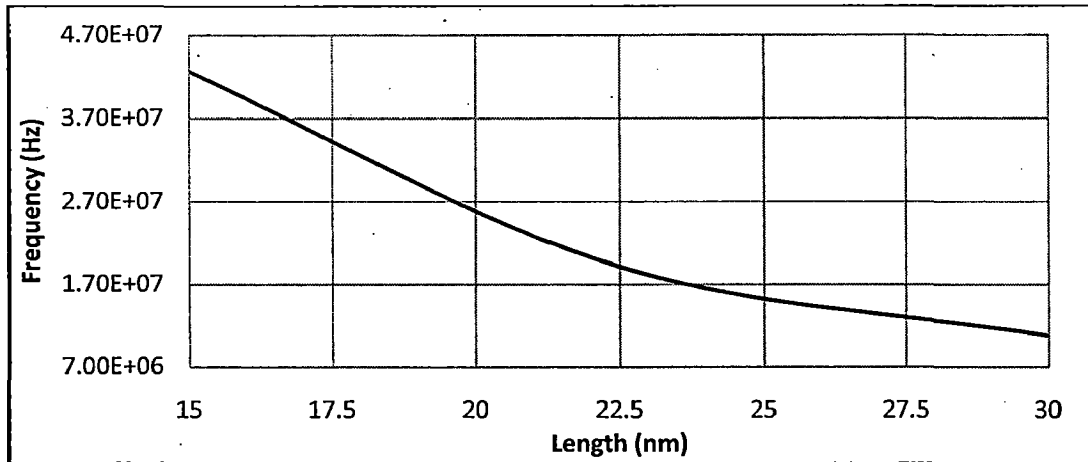


**Fig 5.9:** Effect of change of length on resonant frequency of fixed-free CNT

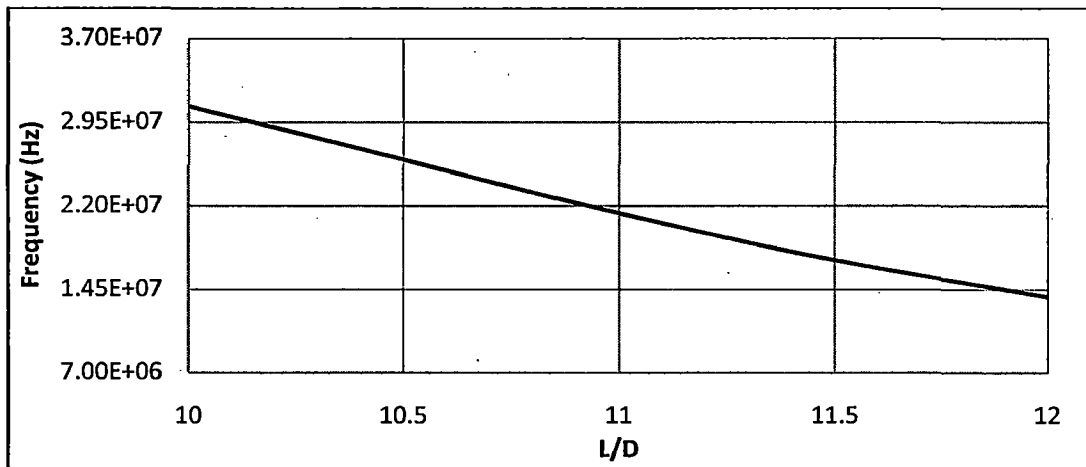


**Fig 5.10:** Effect of change of L/D ratio on resonant frequency of fixed-free CNT

Chirality has its own effect on the frequency of the CNTs. Results shows that for chiral angle ( $0 < \alpha < 30$ ) the harmonic frequency of reduces but for armchair and zigzag are nearly same. Fig 5.11 & 5.12 shows the results for fixed-free and fixed-fixed CNT respectively. Chiral angle has been varied from 0 to 30 degree. For fixed-free CNT frequency values are less as compared to fixed-fixed CNT but the pattern are found to be nearly same. Length of all the CNT is kept 5 nm. CNT used are (9,0), (8,1), (8,2), (7,3), (6,4) and (5,5).

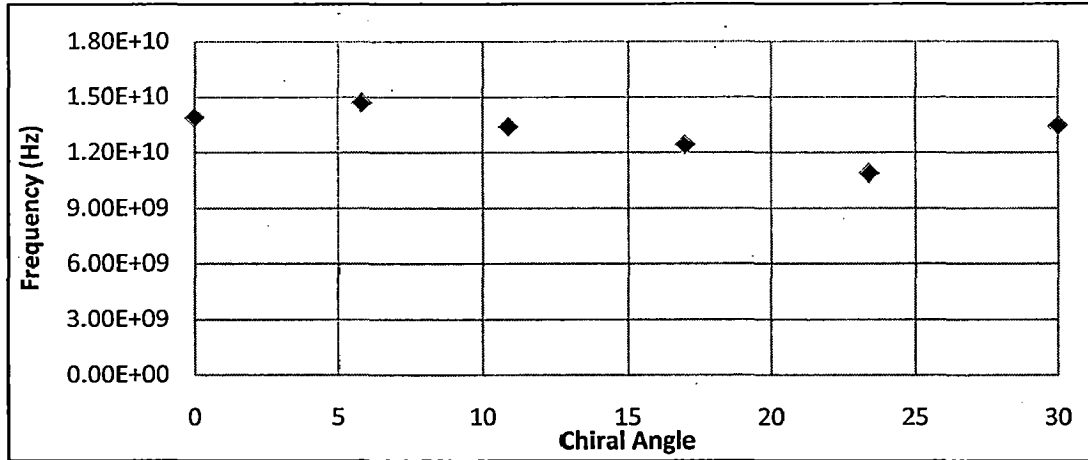


**Fig 5.11:** Effect of chirality on the resonant frequency of fixed-fixed carbon nanotube

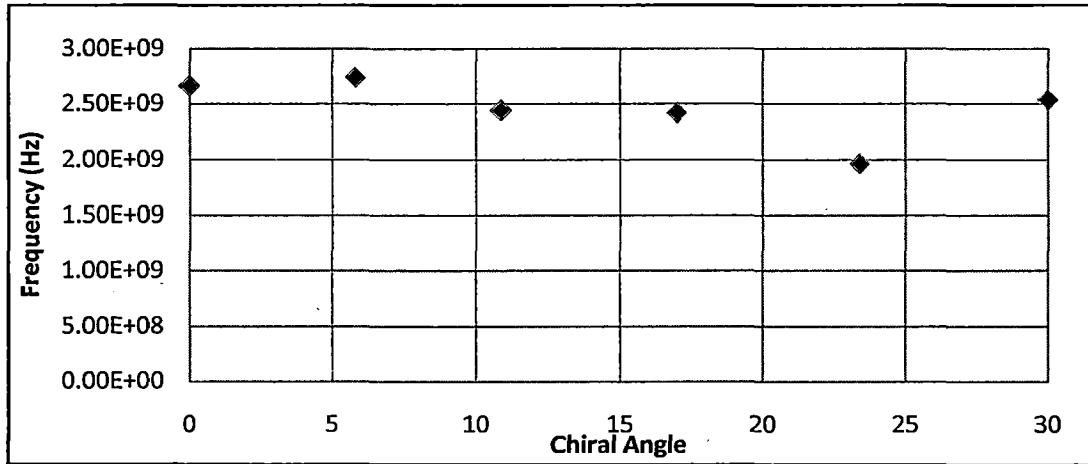


**Fig 5.12:** Effect of chirality on the resonant frequency of fixed-free carbon nanotube

### 5.2.3 WAVINESS

Modelling for waviness is done using continuum mechanics model. FEM results are obtained for both straight and wavy CNTs. Fig 5.13 shows how the frequency changes due to the waviness in the CNT. Results are shown in terms of length variation. Waviness factor ( $e/L$ ) is taken to be 0.1. Fig 5.14 shows that as the waviness of the CNT increases the resonant frequency of the CNT reduces. Diameter & length of CNT for this analysis is taken as 1nm & 20nm respectively. Waviness is varied from 0 to 0.1 and the frequency is observed to be reduced nearly by 9%.

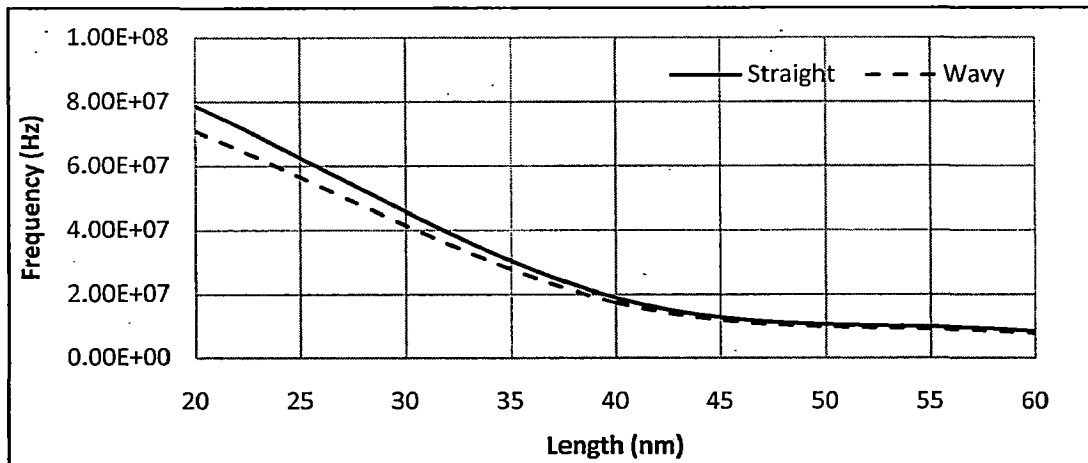


**Fig 5.13:** Comparison between frequency of straight and wavy CNT for various length

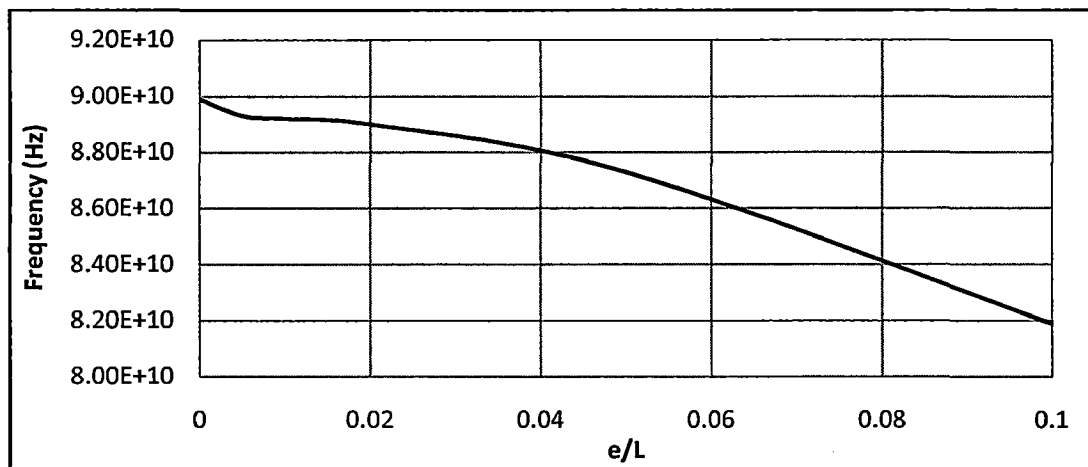


**Fig 5.14:** Variation in frequency due to change in the waviness ( $e/L$ ) of CNT

### 5.2.4 PINHOLE DEFECT

Two type of pinhole defects are taken into consideration (i) Type A (6 atom) and (ii) Type B (24 atom) pinhole defect. It is clear from Fig 5.15 that type B pinhole defect has higher effect on the frequency reduction which is due to the fact that more material removal takes place in case of type B defect than type A. Fig 5.16 shows how frequency reduces for various chiral angles. Pattern observed is the same for defective and non defective CNT. There is a considerable frequency drop for all values of chirality. Frequency drop is nearly constant for most of the chiral angle range. For this analysis the length and diameter of CNT is taken as 50Å and 3.5Å.

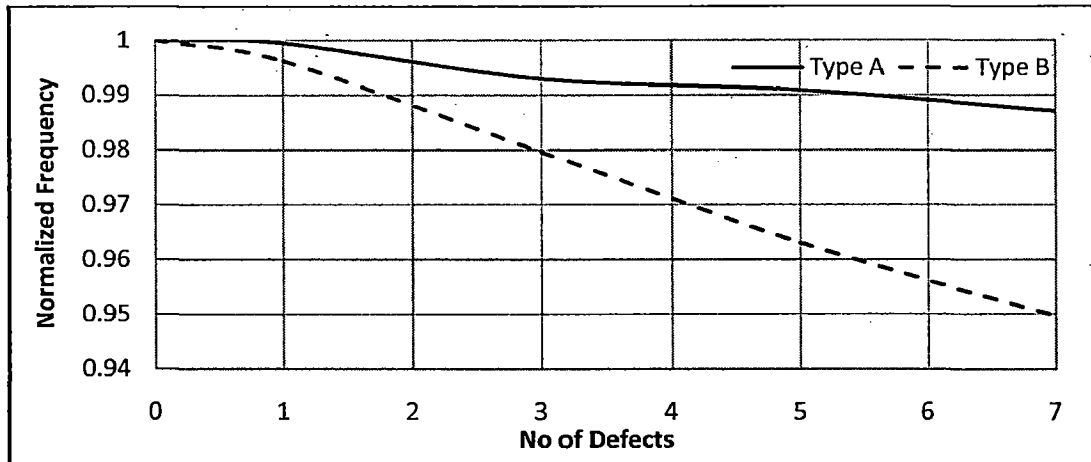


**Fig 5.15:** Frequency ratio (Normalized frequency) for no. of defects for type A and Type B defect in CNT

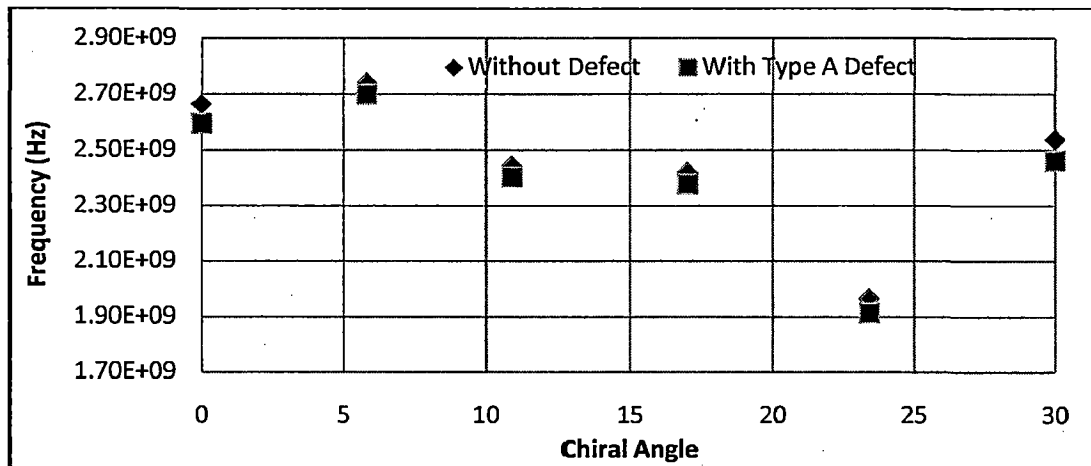


**Fig 5.16:** Change in frequency with change in chiral angle with and without type A pinhole defect in CNT

### 5.2.5 VACANCY DEFECT

For simulating single atom vacancy, defect structural mechanics technique is used. Vacancy defect is studied in cantilever CNT. Fig 5.17 shows the effect of number of defects on the resonant frequency of the CNT. It is clear that frequency reduces as the number of defects increases but it can also be concluded that as the number of defects increases the rate of frequency drop reduces.



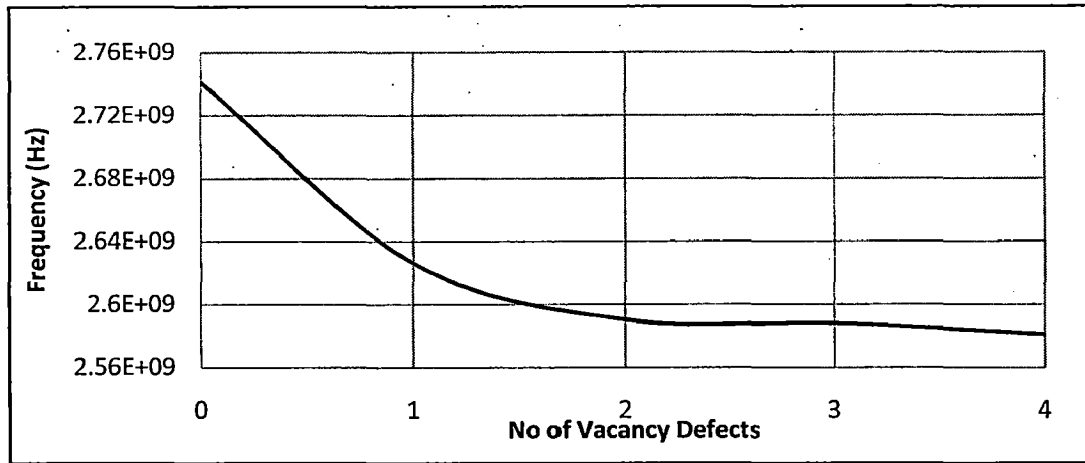


**Fig 5.17:** Change in frequency as no of vacancy defect increases for fixed-free CNT

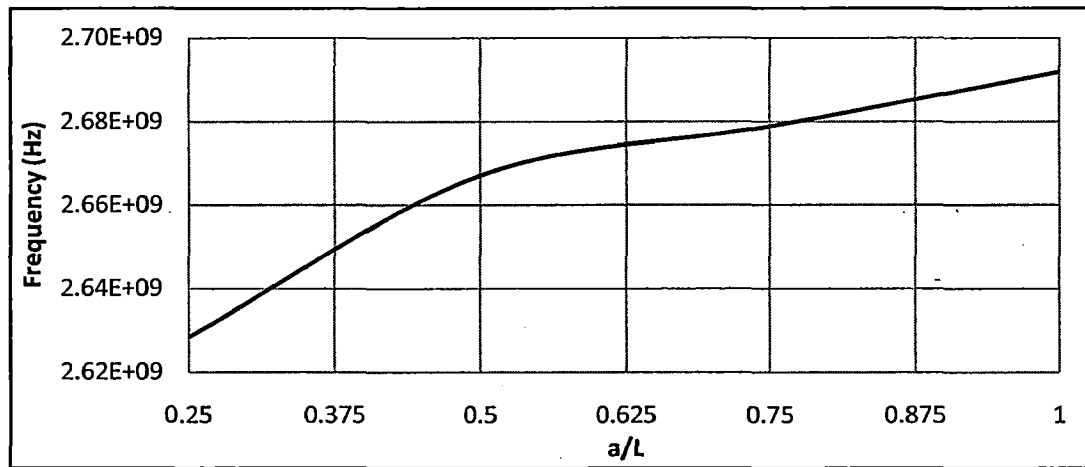


**Fig 5.18:** Change in frequency as vacancy defect moves towards free end in fixed-free CNT

Fig 5.18 predicts the effect of positioning of the vacancy defect. As the single atom vacancy moved towards the free end the frequency increases to the no defect frequency value. Fig 5.19 shows the effect of chirality on the vacancy defect. Defective CNT is taken with 4 single atom vacancy defect placed at regular interval. It is observed that the drop in frequency is constant throughout the range.

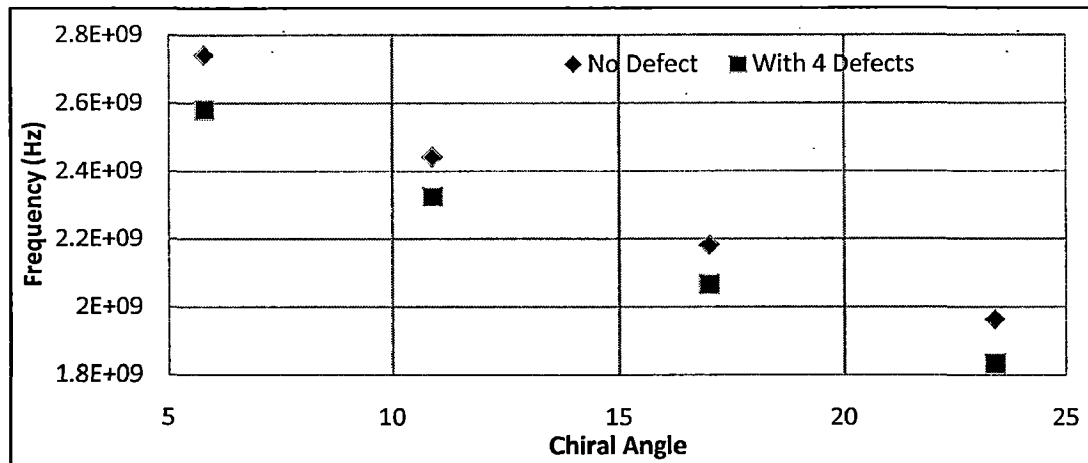


Fig 5.19: Change in frequency as chirality increases CNT with no defect and with 4 defects.

### 5.3 CONCLUSION

From above results and discussion these points can be concluded

- Analytical and FEM results match quite accurately.
- For faultless CNT
  - Higher the diameter higher is the resonant frequency.
  - As the length of the CNT increase the frequency of the CNT reduces.
  - As the L/D ratio increases the frequency of CNT decreases.
  - For chiral angle ( $0 < \alpha < 30$ ) the harmonic frequency of reduces but for armchair and zigzag are nearly same.
- CNT with waviness
  - Wavy CNT have less frequency as compared to straight CNT.
  - As the waviness of the CNT ( $e/L$ ) increases the frequency of the CNT reduces considerably.
- CNT with pinhole defect
  - Two type of artificial defects are taken into consideration Type A (6 atom) and Type B (24 atom) pinhole defect.
  - Due to pinhole defect frequency of the CNT reduces.

- As the number of defects increases frequency of CNT reduces.
- Due to higher material removal Type B pinhole shows higher frequency reduction.
- Defected chiral CNT shows same pattern as faultless CNT but with some frequency reduction.
- CNT with vacancy defect
  - Vacancy defect results in frequency reduction of CNT.
  - As the number of single atom vacancy defects increases frequency of the CNT reduces but reaches toward the saturation.
  - For cantilever CNT as the defect moves towards the fixed end higher frequency reduction takes place.

## **CHAPTER 6**

# **NANOTUBE BASED MASS SENSORS**

Nanobalances based on CNTs have been developed for detection of the masses of extremely tiny particles. Wang et al. [114] reported on the measurement of the mass of a particle as light as 22 fg ( $22 \times 10^{-15}$  g). The measurement was accomplished by observing the resonance frequency shift of a CNT nanocantilever under a transmission electron microscope (TEM) after the mass is attached to the tip of the CNT, as shown in Fig 6.1. Li and Chou [89] applied their molecular structural mechanics approach to study the frequency shifts in cantilevered and bridged SWNTs with attached particles. The two cases are shown schematically in Fig 6.2. It was predicted that mass sensitivity of such CNT nanobalances can reach  $10^{-21}$  g, and that a logarithmically linear relationship exists between the resonant frequency and the attached mass when the mass is larger than about  $10^{-20}$  g. Absorption of gases or fluids by CNTs can also cause the CNT resonance frequencies to shift, and this phenomenon has opened up a new area of research on CNT-based sensors [115–120].

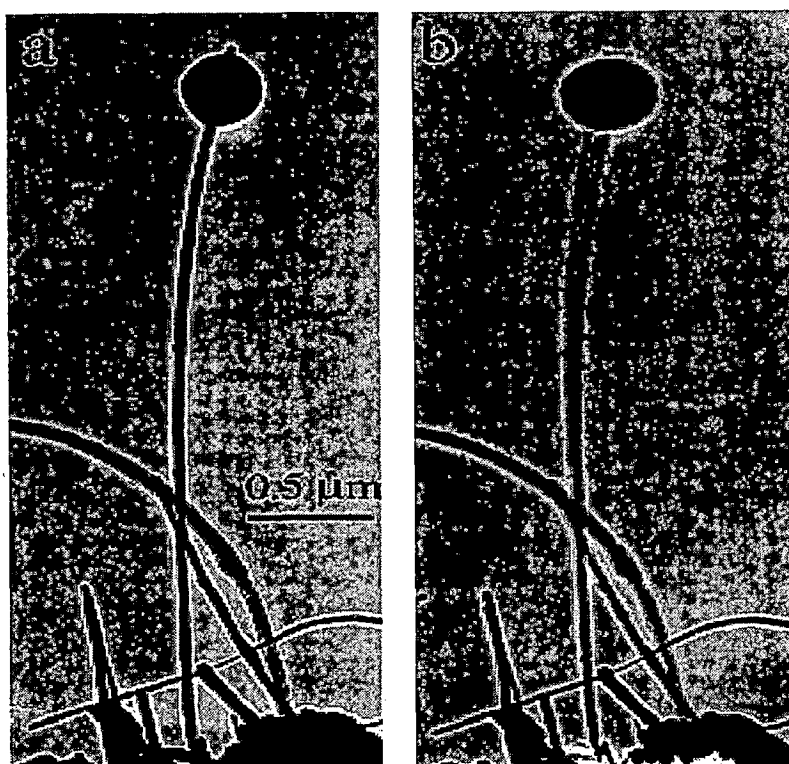


**Fig 6.1:** TEM photographs of a small particle attached at the end of a CNT nanocantilever vibrating at first harmonic resonance frequency [114].

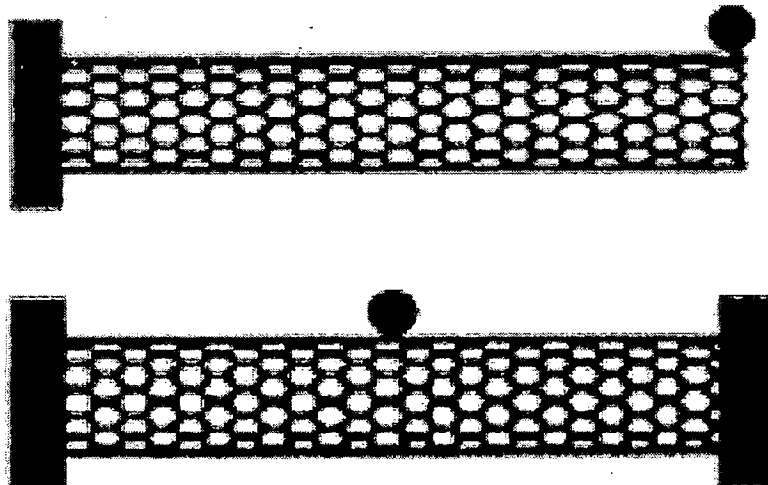


**Fig 6.2:** Cantilevered and bridged nanotube resonator with an attached mass [89].

Recently researchers used carbon nanotubes to weigh individual gold atoms [121]. The Fig 6.3 shows a nanotube oscillating at a constant frequency set by a radio wave. As atoms land on the nanotube, the frequency of the oscillation decreases. This change can be used to calculate the weight of the atoms.

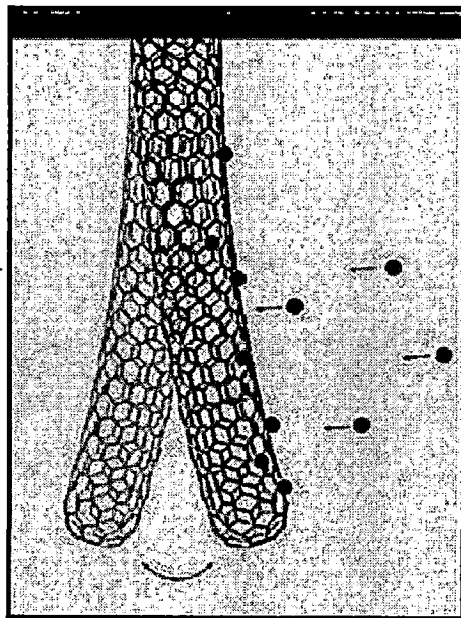


**Fig 6.3:** Cantilever SWCNT used as a atom mass sensor

## 6.1 ANALYTICAL METHODS

### 6.1.1 RESONANT FREQUENCIES WITH ATTACHED MASS

The continuum models based on beam as well as shell have been used extensively for single- and multi-walled carbon nanotubes. In order to obtain simple analytical expressions of the mass of attached biochemical entities, we model a single-walled CNT using a rod based on the Euler–Bernoulli beam theory. The equation of motion of free-vibration can be expressed as

$$EI \frac{\partial^2 y}{\partial x^2} + \rho A \frac{\partial^2 y}{\partial t^2} = 0$$

where  $E$  is Young's modulus,  $I$  the second moment of the cross-sectional area  $A$ , and  $\rho$  the density of the material. Suppose the length of the SWCNT is  $L$ . Depending on the boundary condition of the SWCNT and the location of the attached mass, the resonant frequency of the combined system can be derived. We only consider the fundamental resonant frequency, which can be expressed as

$$f_n = \frac{1}{2\pi} \sqrt{\frac{k_{eq}}{m_{eq}}}$$

Here  $k_{eq}$  and  $m_{eq}$  are respectively equivalent stiffness and mass of SWCNT with attached mass in the first mode of vibration. Two kinds of end constraints, i.e., cantilever and bridged, are considered.

### 6.1.2 CANTILEVER CNT WITH MASS AT THE TIP

Mass ( $M$ ) is attached at free end. For this case it can be shown that  $F_{eq} = 3EI/L^3$  so that

$$k_{eq} = \frac{3EI}{L^3}$$

$$m_{eq} = \frac{33}{140} \rho AL + M$$

The resonant frequency can be shown as

$$f_n = \frac{1}{2\pi} \sqrt{\frac{k_{eq}}{m_{eq}}} = \frac{1}{2\pi} \frac{\alpha^2 \beta}{\sqrt{1 + \Delta M}}$$

where

$$\alpha = 1.888, \beta = \sqrt{\frac{EI}{\rho AL^4}} \text{ and } \Delta M = \frac{140}{33} \cdot \frac{M}{\rho AL}$$

The relationship between the resonant frequencies can be written as

$$f_n = \frac{f_0}{\sqrt{1 + \Delta M}}$$

### 6.1.3 BRIDGED CNT WITH MASS AT THE MIDPOINT

The present study considers the case of a doubly clamped SWCNT with a nano-scale particle attached to its mid position. The minimum detectable mass change of the sensor can be approximated by the formula

$$f_{res} = \frac{1}{2\pi} \sqrt{\frac{k_{eq}}{m_{eq}}}$$

where  $k_{eq} = \frac{192EI}{L^3}$  &  $m_{eq} = \frac{13}{35}\rho AL + M$

where I is the moment of inertia,  $\rho$  is the density, A is the area, L the length, and E is the Young's modulus of the SWCNT and M is the mass of the attached nanoparticle.

The wavy carbon nanotube resonator under investigation is schematically shown in Fig 6.4. It is described as a beam with an annular cross section having a large aspect ratio. The nano beam is considered doubly clamped and has a sinusoidal curvature with a small rise function described by

$$Z = e \cdot \sin \frac{\pi \cdot x}{l}$$



where  $x$  is the spatial coordinate,  $L$  is the length of the carbon nanotube and  $e$  is the amplitude of its waviness.

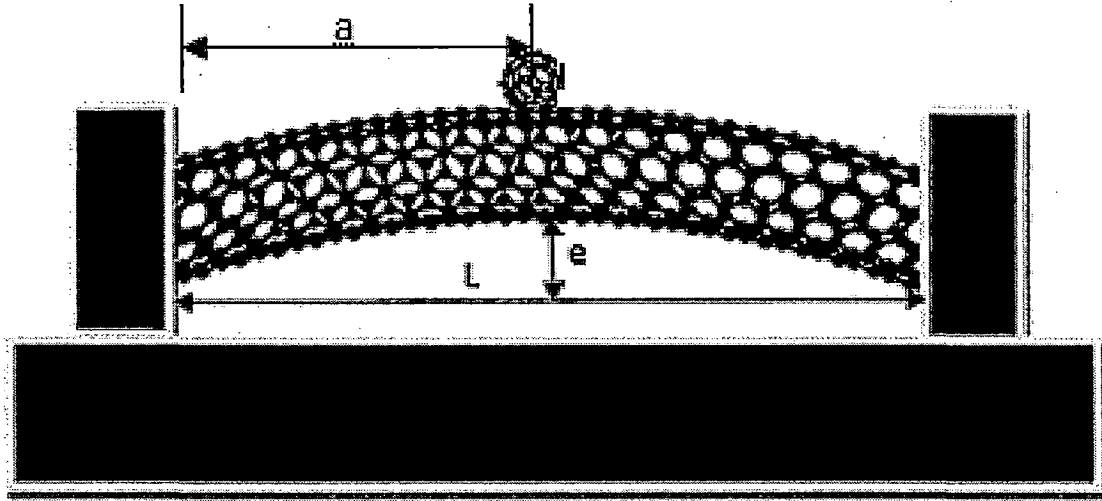


**Fig 6.4:** Configuration of Carbon Nanotube resonator having waviness defined by ratio  $e/L$  and mass attached at position 'a'

## 6.2 RESULTS & DISCUSSIONS

### 6.2.1 ANALYTICAL VS FEM

Analytical as well as FEM results are computed for both cantilever and bridged CNT. Fig 6.5 shows that FEM and analytical results are approximately same and vary by maximum of 5.5%. Fig 6.5 shows the frequency variation for various lengths for a cantilever CNT with diameter of 1.1nm. Mass is attached at the tip of free end of CNT. Mass is taken to be  $10^{-22}$  Kg. Fig 6.6 Shows the same results but for a bridged CNT and mass ( $10^{-20}$  Kg) is attached at the mid of the CNT. Length of the CNT is varied from 20nm to 60nm and diameter is taken as 1.1nm. Results between analytical and FEM are found to be varied by approximately maximum of 6.5%.

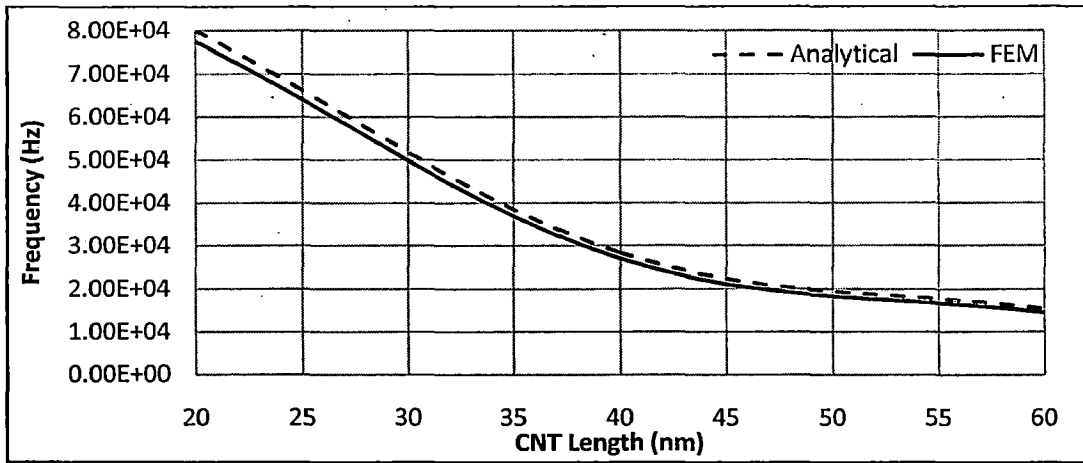


**Fig 6.5:** Comparison of analytical and FEM results for Fixed-free CNT

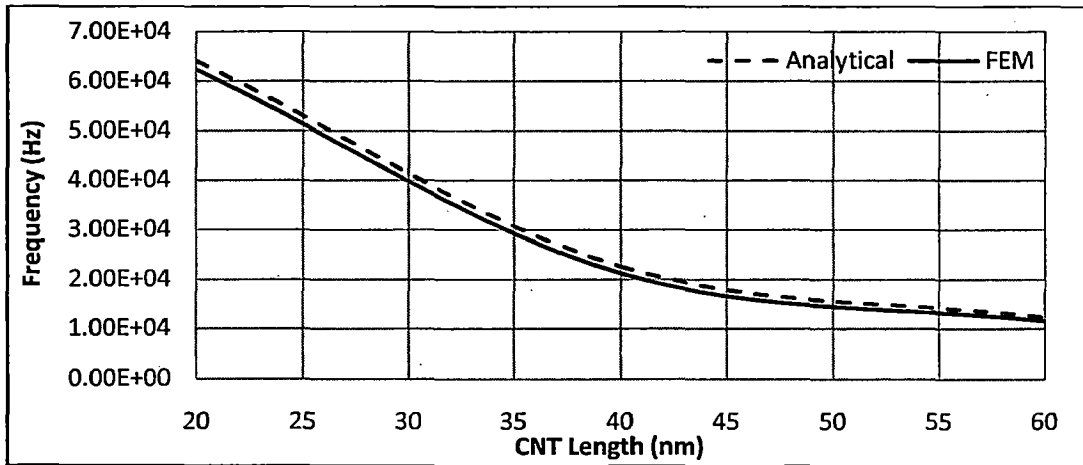
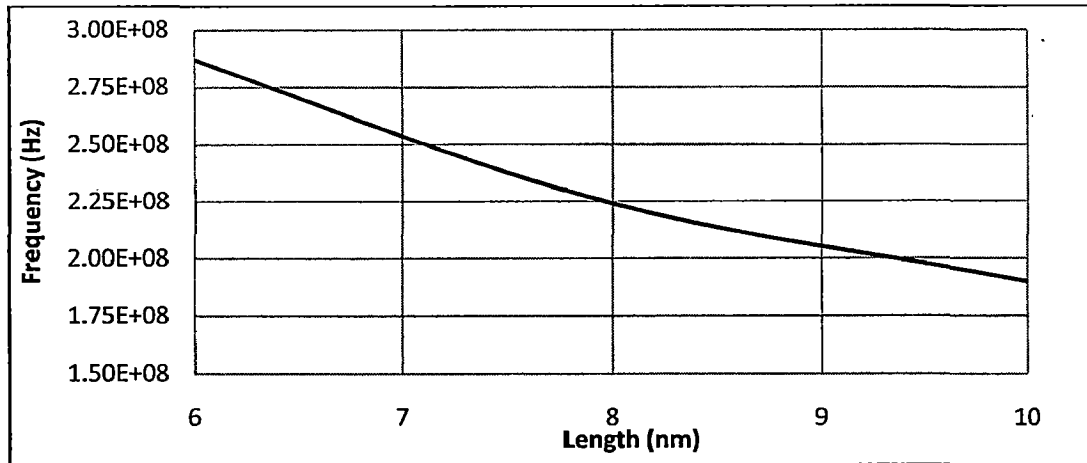


**Fig 6.6:** Comparison of analytical and FEM results for Fixed-fixed CNT

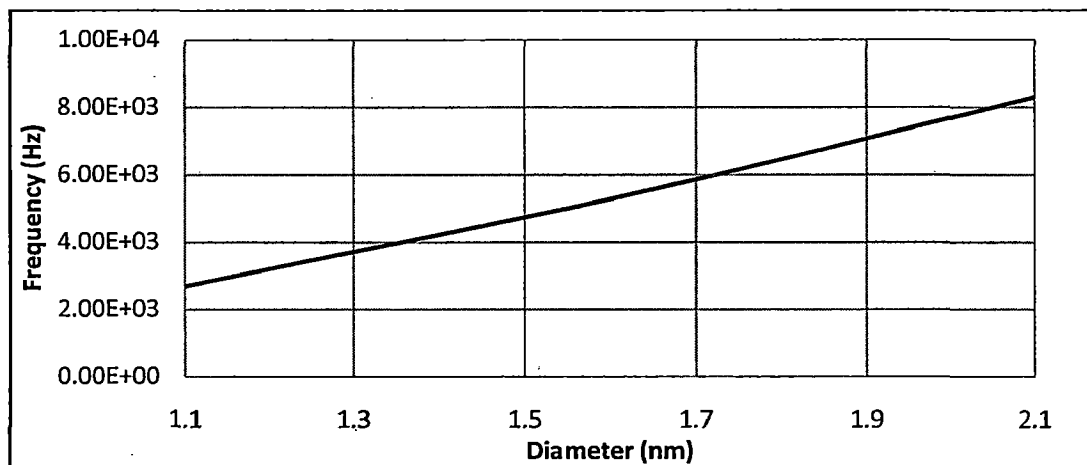
### 6.2.2 WITHOUT DEFECTS

Fig 6.7 & Fig 6.8 shows the same pattern of frequency variation with change in length and diameter as for nanomechanical resonator in previous chapter. Length of the CNT is varied from 6nm to 10nm and diameter is kept constant at 0.8nm and mass ( $10^{-20}$  Kg) is kept at the tip of the free end of CNT. Diameter in Fig 6.8 is varied from 1.1nm to 2.1 nm where length of CNT is taken as 40nm. Mass of  $10^{-20}$  Kg is attached at the tip of the free end. Fig 6.9 shows the effect of the value of mass attached at the tip. It is clear from the Fig 6.9 that as the value of mass increases the resonant frequency reduces considerably. Mass attached is varied

from  $10^{-25}$  Kg to  $10^{-20}$  Kg. Fig 6.11 & Fig 6.12 shows the effect of change of position of mass along the length of cantilever and doubly clamped CNT respectively.



**Fig 6.7:** Effect of change of length on the frequency of fixed-free CNT



**Fig 6.8:** Effect of change of diameter on the frequency of fixed-free CNT

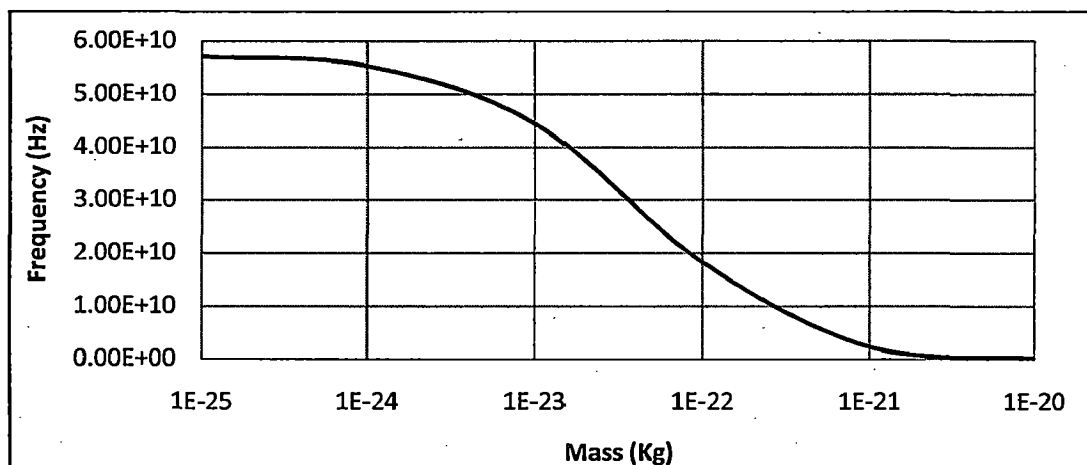


**Fig 6.9:** Change in frequency of mass sensors as mass at tip change in a fixed-free CNT

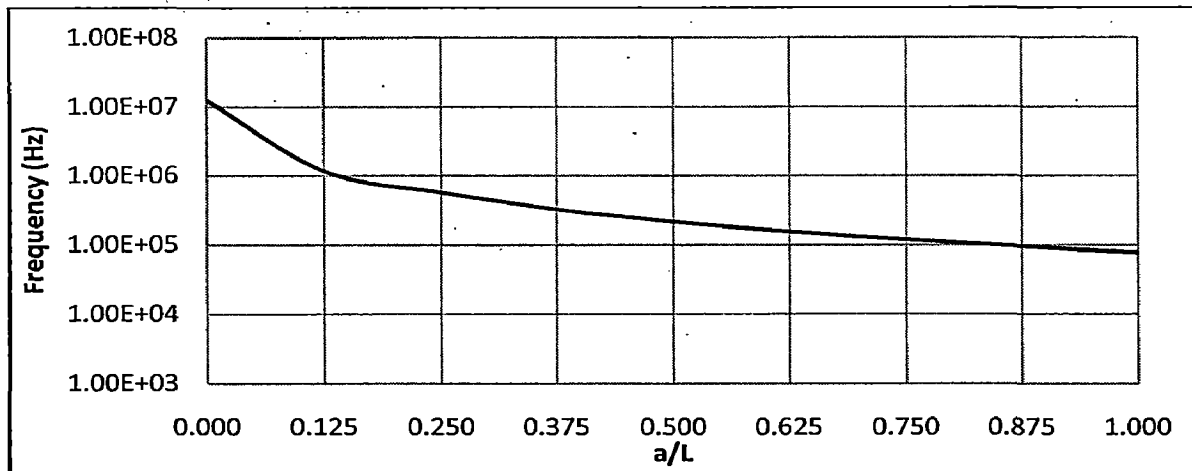


**Fig 6.10:** Effect of the change of position of mass along the length of a fixed-free CNT

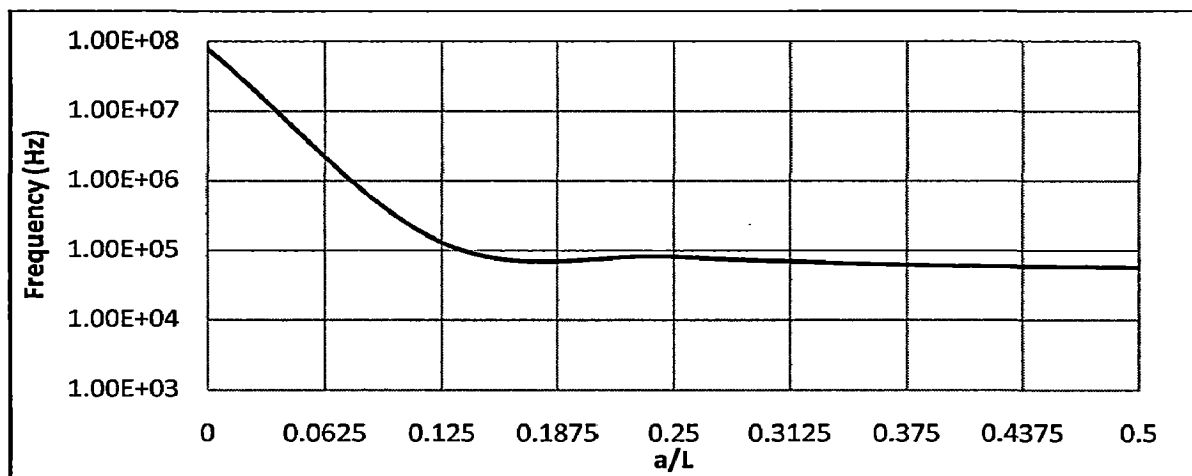
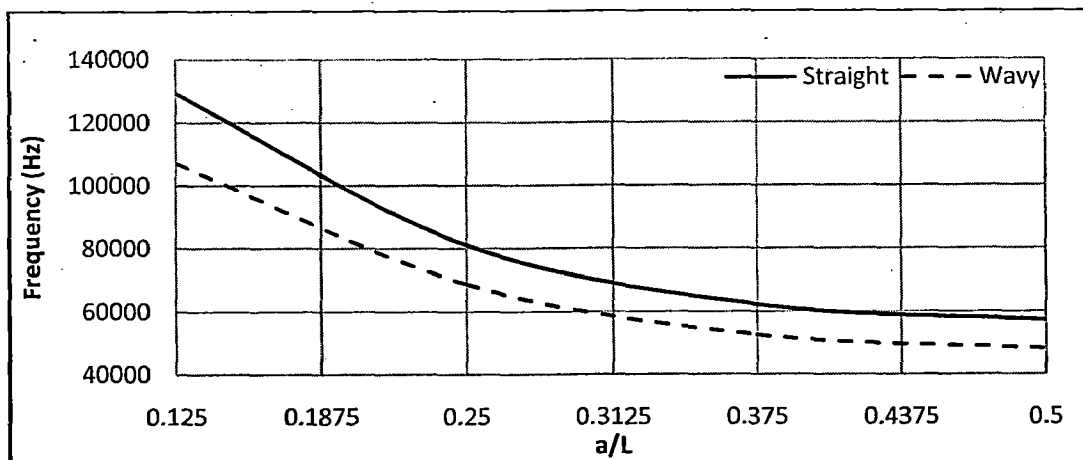


**Fig 6.11:** Effect of the change of position of mass along the length of a fixed-fixed CNT

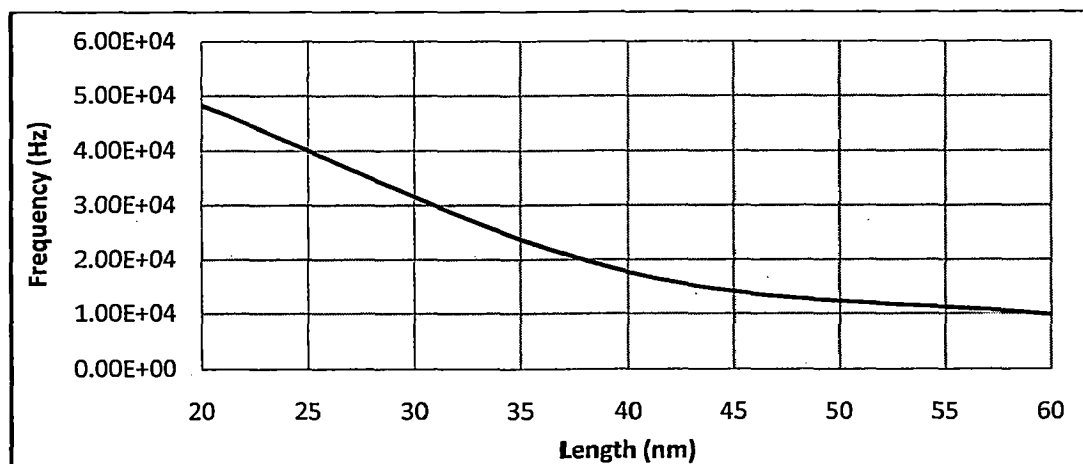
It is observed that in case cantilever CNT as the mass moves towards the free end the frequency of the CNT reduces. In case of bridged CNT as the mass moves toward the mid of length the frequency reduces.

### 6.2.3 WAVINESS

Fig 6.13 shows the FEM results for both straight and wavy CNT. Mass of  $10^{-20}$  Kg is attached at various position of the CNT. Length and diameter of the bridged CNT are taken as 20 nm and 1.1 nm respectively. Wavy CNT shows the same pattern as the straight CNT but the frequency of wavy CNT is less than the straight CNT.



**Fig 6.12:** Effect of  $a/L$  on the frequency for straight and wavy fixed-fixed CNT



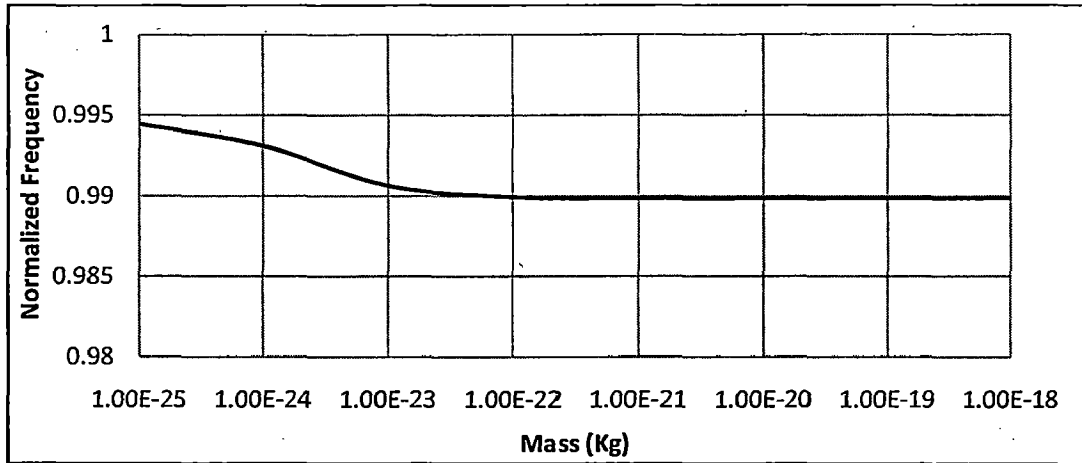
**Fig 6.13:** Change in Frequency with increase in length of a fixed-fixed CNT

Fig 6.14 shows the variation of resonant frequency with the increase in the CNT length. Length of the CNT is varied from 20nm to 60nm. Mass of  $10^{-20}$  Kg is attached at the mid length of the CNT. Diameter of CNT is considered to be 1.1nm. All above results related to wavy CNT are computed for waviness factor ( $e/L$ ) equal to 0.1. Like straight CNT in CNT with waviness shows the same effect. As the length of the CNT increases the frequency reduces.

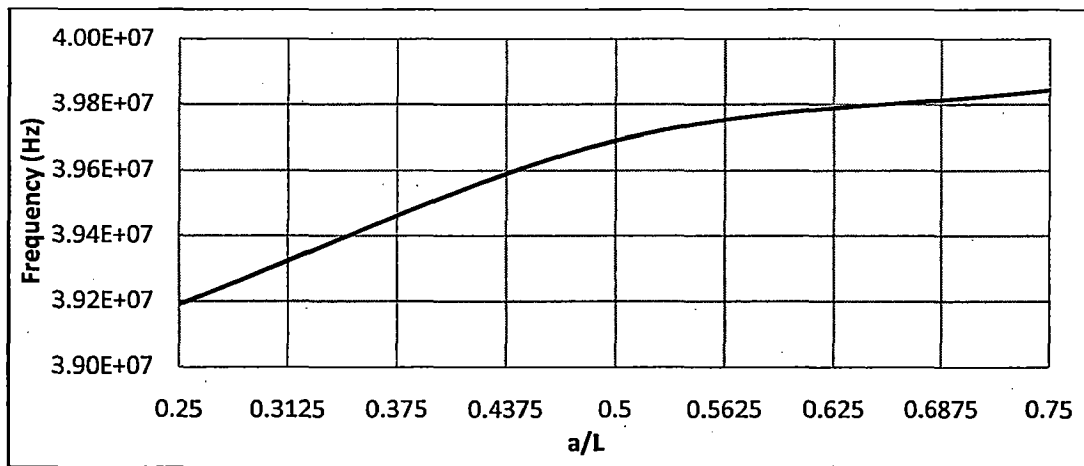
### 6.2.4 VACANCY DEFECT

Effect of vacancy defect on mass sensors is studied using the structural mechanics technique.

Fig 6.15 shows the normalized frequency for different value of mass from  $10^{-25}$  Kg to  $10^{-18}$  Kg. It can be concluded that as the mass increases the effect of single atom vacancy defect stabilizes.



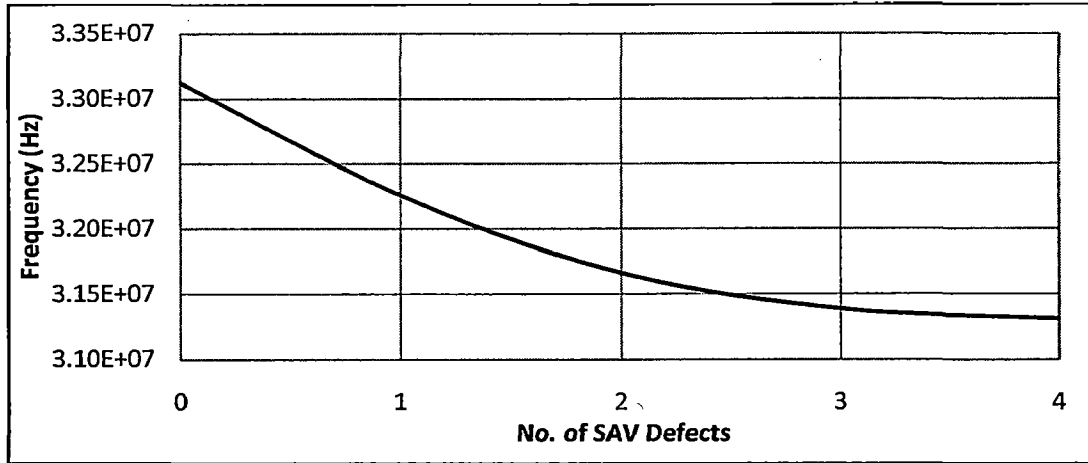
**Fig 6.14:** Change in Normalized frequency ( $F_{sav}/F$ ) of mass sensor for different masses for a fixed-free CNT



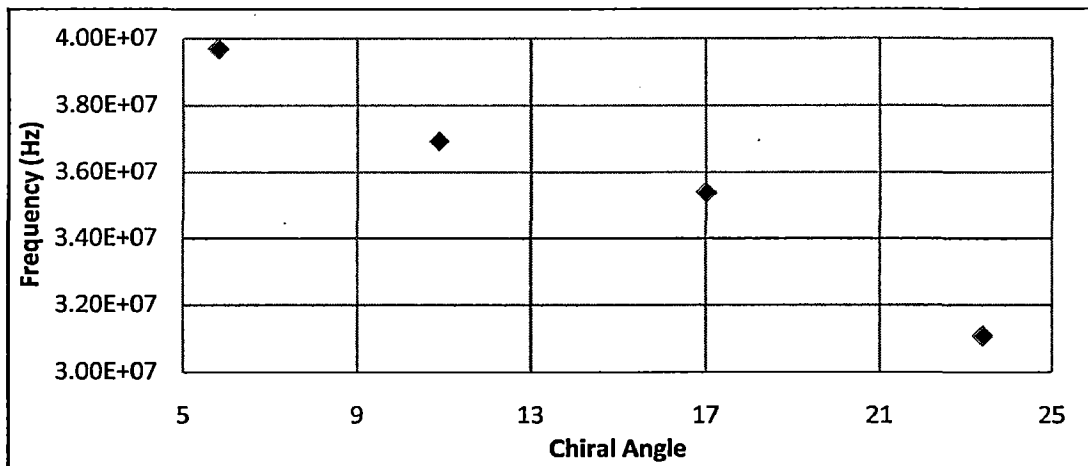
**Fig 6.15:** Effect of change in position of SAV in a fixed-free CNT

Fig 6.16 shows change in frequency as the position of the single atom vacancy changes. (8,1) CNT is used for the analysis with  $10^{-20}$  Kg mass. Length of the CNT is taken as 50nm. It can be observed that as the single atom vacancy defect moves towards the free end the frequency

of the CNT increases. Fig 6.17 depicts the decrease in the frequency as the number of vacancy defect increases. For higher values of vacancy defect the drop in the frequency saturates. As it can be observed that frequency for 3 SAV defects and for 4 SAV defects are nearly same.



**Fig 6.16:** Change in frequency as the number of defects increases in a fixed-free CNT



**Fig 6.17:** Effect of chirality on the mass sensors with SAV defect in a fixed-free CNT

Effect of chirality can be shown from Fig 6.18. As the chiral angle increases the frequency of CNT with SAV defect reduces. Results are shown for mass of  $10^{-20}$  Kg and 50 nm length.

## 6.3 CONCLUSIONS

From above results and discussion these points can be concluded

- Analytical and FEM results vary just by maximum of 6.5%.
- For faultless CNT
  - Higher the diameter higher is the resonant frequency.
  - As the length of the CNT increase the frequency of the CNT reduces.
  - As the value of mass increase the frequency of CNT reduces.
  - In cantilever CNT as the attached mass moves towards the free end the frequency of the CNT reduces.
- CNT with waviness
  - Wavy CNT based mass sensors have less frequency as compared to straight CNT.
  - As the length of the CNT based mass sensors increases the frequency reduces.
- CNT with vacancy Defect
  - Vacancy defect results in frequency reduction of CNT based mass sensors.
  - As the mass increases the effect of single atom vacancy defect stabilizes.
  - As the single atom vacancy defect moves towards the free end the frequency of the CNT increases
  - As the number of single atom vacancy defects increases frequency of the CNT reduces but reaches toward the saturation.
  - As the chiral angle increases ( $5 < \alpha < 25$ ) the frequency of CNT with SAV defect reduces.



## **CHAPTER 7**

# **CARBON NANOTUBE FRACTURE**

Nanoscale fracture experiments and simulations demonstrate the potential to probe and exploit the ultimate strength of materials [66, 122-128]. These studies also point to the need for an understanding of the mechanisms governing the formation and extension of nanometer-sized cracks in a broad range of fields and applications [129-133]. Researchers have studied the tensile fracture [134] and C-chain unravelling in CNTs by molecular dynamics (MD) simulations, suggesting that CNTs have an extremely large breaking strain (>30%). Contrastively, some argued, also based on results of MD simulations that CNT fracture depends primarily on the inflection point on the curve of interatomic potential of the C-C bond and predicted that their fracture strain ranged between 10 and 19%. So far, predictions of CNT failure, in which the atomic structure is always assumed defect-free at the beginning, are limited to yielding and fracture behaviours at relatively high strain levels (>5%) [135]. All these hypotheses apply to transient behaviours of CNTs under critical conditions. However, in actual applications CNTs will most likely be loaded at much lower strain rates so here we have studied how various CNT parameters like length, diameter, fracture position and crack orientation affect the fracture vulnerability of a CNT. In this chapter the Fracture Mechanics approach is used on solid model of CNT to calculate factors like Stress Intensity Factors (SIFs) and J Integral (J).

## **7.1 FRACTURE MECHANICS**

Experimental observations and theoretical elasticity helped to create the fundamental aspects of the theory of fracture mechanics. Major differences between the theoretical prediction of tensile strength and the experimentally measured one is the assumption of existing minute flaws and defects; predicting drastic changes in the distribution of the stress field around each flaw, regardless of its actual size. The fundamental concepts of stress intensity factor, energy release rate, etc. are used to analyze a crack problem. Energy based methods allows the classical fracture mechanics to be extended to nonlinear problems. SIF & J integral are

powerful numerical tools to be used for efficiently determining the necessary fields and variables [136].

### 7.1.1 STRESS INTENSITY FACTOR (SIF)

The stress intensity factor is a fundamental quantity that governs the stress field near the crack tip. It can be used to predict the failure of a cracked plate. The stress intensity factor depends on both the geometrical configuration and the loading conditions of the body. These load types are categorized as Mode I, II, or III. Stress intensity in any mode situation is directly proportional to the applied load on the material. Irwin [137] introduced the concept of stress intensity factor defined as:

$$K_I = \lim_{r \rightarrow 0, \theta = 0} \sqrt{2\pi r} \sigma_{22}$$

$$K_{II} = \lim_{r \rightarrow 0, \theta = 0} \sqrt{2\pi r} \sigma_{12}$$

$$K_{III} = \lim_{r \rightarrow 0, \theta = 0} \sqrt{2\pi r} \sigma_{23}$$

where  $\sigma_{ij}$  are the near crack tip stresses, and  $K_i$  are associated with three independent kinematic movements of the upper and lower crack surfaces with respect to each other, as shown in Fig 7.1.

**Opening Mode, I:** The two crack surfaces are pulled apart in the y direction, but the deformations are symmetric about the x - z and x - y planes.

**Shearing Mode, II:** The two crack surfaces slide over each other in the x-direction, but the deformations are symmetric about the x - y plane and skew symmetric about the x - z plane.

**Tearing Mode, III:** The crack surfaces slide over each other in the z-direction, but the deformations are skew-symmetric about the x - y and x - z planes.

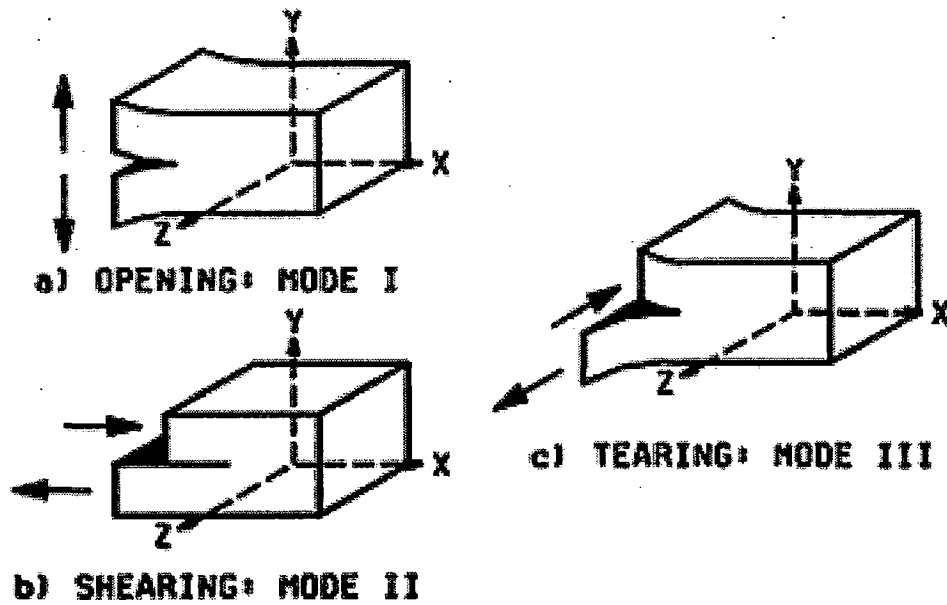


Fig 7.1: Independent Fracture Modes

The SIF is the measure of the strength of the singularity. One of the underlying principles of Fracture Mechanics is that unstable fracture occurs when the SIF reaches a critical value  $K_{Ic}$ .  $K_{Ic}$  or fracture toughness represents the inherent ability of a material to withstand a given stress field intensity at the tip of a crack and to resist progressive tensile crack extensions.

### 7.1.2 J- INTEGRAL (J)

The J-integral is widely accepted as a fracture mechanics parameter for both linear and nonlinear material response. It is related to the energy release associated with crack growth and is a measure of the intensity of deformation at a notch or crack tip, especially for nonlinear materials [138-139]. If the material response is linear, it can be related to the stress intensity factors. Because of the importance of the J-integral in the assessment of flaws, its accurate numerical evaluation is vital to the practical application of fracture mechanics in design calculations. In the context of quasi-static analysis the J-integral is given as

$$J = \lim_{z \rightarrow 0} \int n.H.q.dz$$

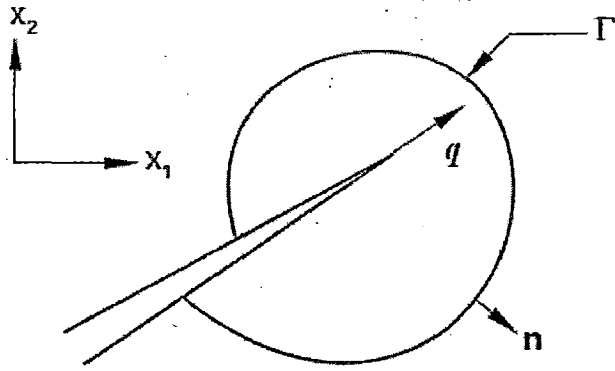


Fig 7.2: J-Integral in two dimensions

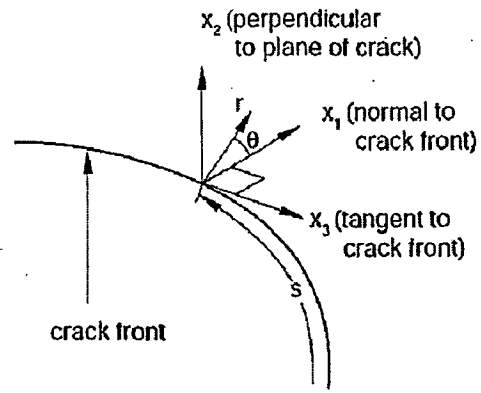


Fig 7.3: J- Integral in three dimensions

As shown in Fig 7.2, the ‘ $\Gamma$ ’ is a contour beginning on the bottom crack surface and ending on the top surface, ‘ $q$ ’ is a unit vector in the virtual crack extension direction and ‘ $n$ ’ is the

outward normal to  $\Gamma$ .  $H$  is given by  $H = WI - \sigma \frac{\partial u}{\partial x}$ .

For elastic material behaviour,  $W$  is the elastic strain energy; for elastic-plastic or elastic-visco plastic material behaviour the  $W$  is defined as the elastic strain energy density plus the plastic dissipation, thus representing the strain energy in an “equivalent elastic material.”

The J-integral can be extended to three dimensions (as shown in Fig 7.3) by considering a crack with a tangentially continuous front. The local direction of virtual crack extension is again given by  $q$ , which is perpendicular to the local crack front and lies in the crack plane. Asymptotically, as  $r \rightarrow 0$ , the conditions for path independence apply on any contour in the  $x_1$ - $x_2$  plane, which is perpendicular to the crack front at  $s$ . For a virtual crack advance in the plane of a three-dimensional crack, the energy release rate is given by

$$\bar{J} = \int_{\Gamma} J(s) \lambda(s) ds$$

$$\bar{J} = \lim_{z \rightarrow 0} \int_{At} \lambda(s) n \cdot H \cdot q \cdot dA$$

## 7.2 RESULTS & DISCUSSIONS

Simulation results are shown in normalized form as the purpose of this simulation is to generate the results and to have an understanding for which combinations of length, diameter, position and orientation crack is more vulnerable. For obtaining the results strain of 5% is applied to the CNT.

Fig 7.4 shows that there is no effect of length on the probability of crack propagation in CNT. Both the values of J integral and Stress intensity factor are constant. In this case crack is taken to be perpendicular to the length of CNT and considered to be in the middle of the length. Diameter of CNT is taken as 1.1nm.

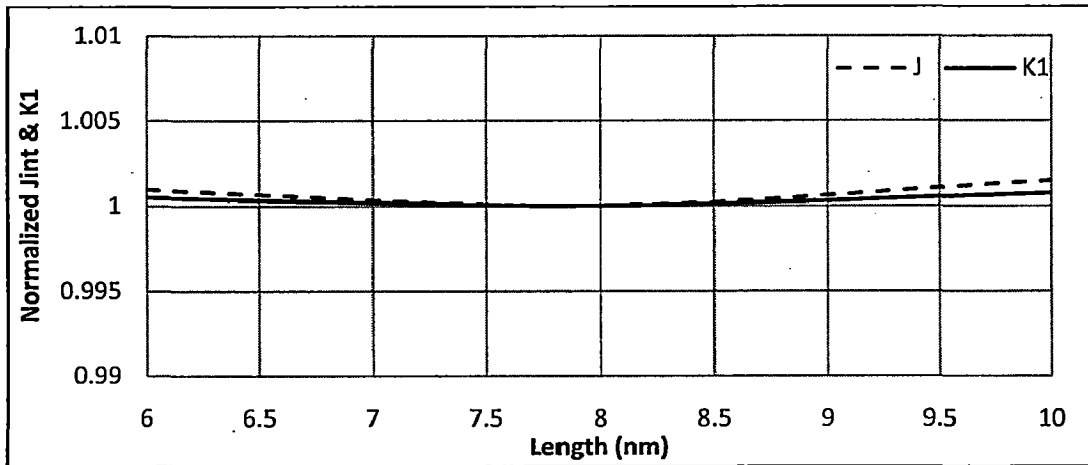


Fig 7.4: Effect of CNT Length on the J and K1

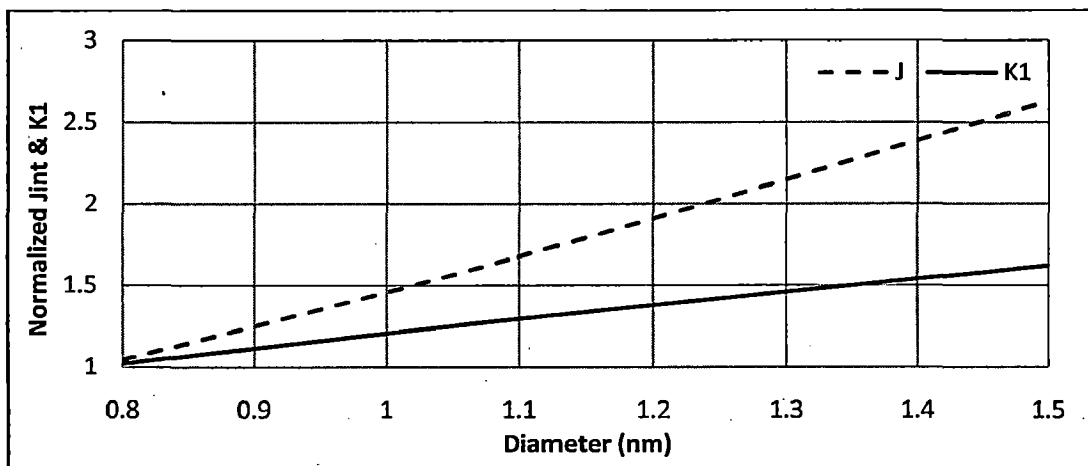


Fig 7.5: Effect of CNT diameter on the J and K1

Fig 7.5 shows the variation of J integral and SIF value as the diameter of the CNT increases. Unlike the length as the diameter of CNT increases the J integral and SIF value increases significantly. So it can be seen that as the diameter of CNT increases the chances of crack propagation increases for same crack length to diameter ratio. Results in Fig 7.6 shows that J integral and SIF value are higher if the crack is nearer to the mid length. This depicts that crack in mid section of a CNT have more chances of propagating than other positions. Crack orientation also shows some changes in crack vulnerability. Fig 7.7 shows as the chiral angle increases the SIF ( $K_2$ ) and J values increases. It observed that values of SIF ( $K_1$ ) do not change much. This clearly shows that at higher chiral angle, the chance of crack propagation is higher.

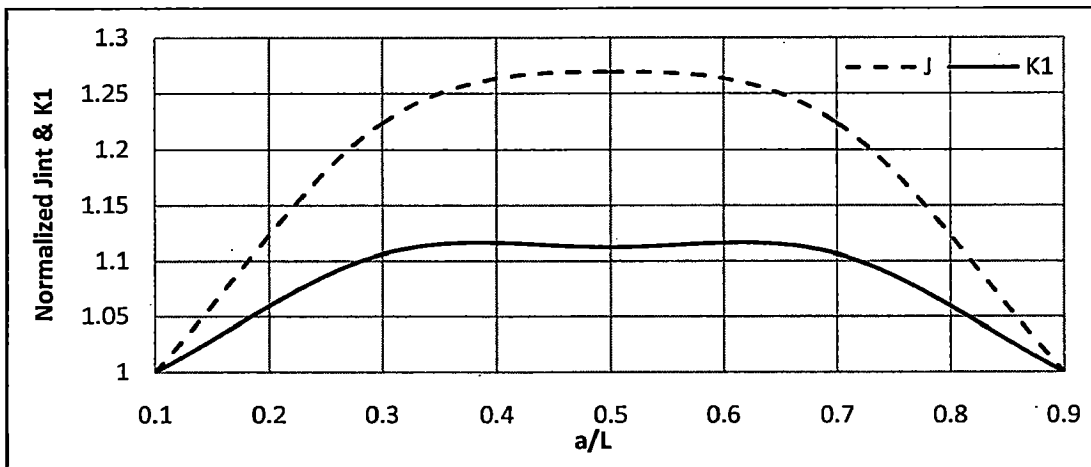


Fig 7.6: Effect of crack position on the J & K1 of CNT

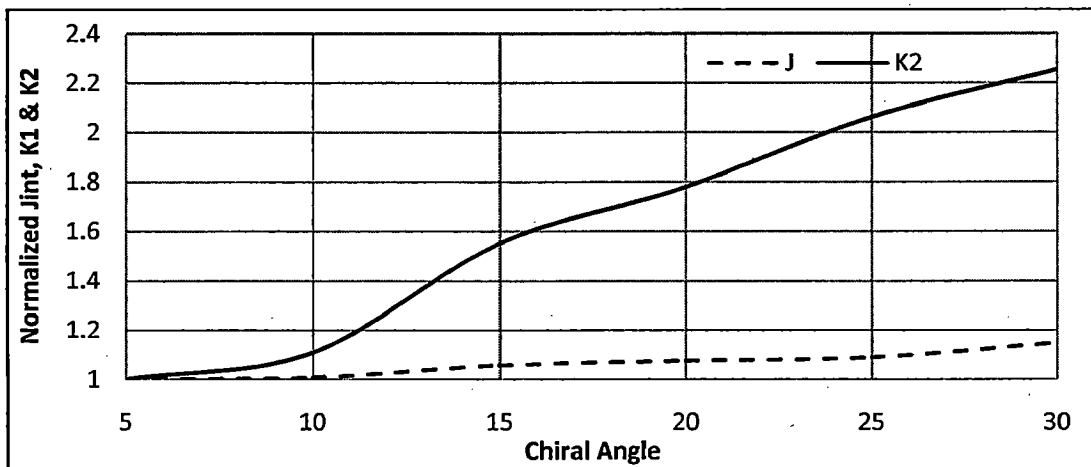


Fig 7.7: Normalized J,  $K_1$  and  $K_2$  values for different chiral angle

### 7.3 CONCLUSIONS

From simulation results using continuum mechanics following conclusion can be drawn

- Fracture mechanics approach is used to simulate the crack in CNT.
- J Integral and Stress Intensity Factor are computed as a measure of crack propagation.
- There is no effect of length on the crack propagation.
- As the diameter of CNT increases the chances of crack propagation increases for same crack length to diameter ratio.
- If crack in mid section of the, it CNT have more chances of propagating.
- At higher chiral angle the chance of crack propagation is higher.



**CHAPTER 8**

**CONCLUSION & FUTURE SCOPE**

## 8.1 CONCLUSIONS

This report contains the effect of various defects in Carbon Nanotube frequency characteristics. The results of this report can be concluded as follows:

- Continuum mechanics and structural mechanics (beam element) techniques are used for simulation and modelling of carbon nanotube.
- FEM software ABAQUS is used as a finite element tool to simulate the results.
- Analytical model and FEM model are compared and results are found to be close enough.
- Three important mechanical applications are taken into consideration under this study and they are as follows:
  - Nanomechanical Resonators
  - Nanotube based Mass sensors
  - CNT as a structural element
- Various faults and the effect of chirality are taken into account. Different defects that are considered are waviness, vacancy defect, pinhole defect and crack in CNT.
- It is observed that defects discussed in this report reduces the resonant frequency on CNT & the reduction differs for various combination of CNT, defect type and location of defect.
- Different combination of CNT like length, diameter and positioning of mass or defects are considered.
- For the case of frequency analysis chirality, waviness, pinhole and vacancy defects are considered.
- For the case of stress analysis chirality and crack are considered for fault analysis.
- Results are explained and the variation of the frequency is characterised based on various variables and factors.

## 8.2 FUTURE SCOPE

Nanotechnology is emerging technology with a lot of future promises. A lot of work can be done in future related to this project. Some of them are as follow:

- Various other simulation and modelling techniques like molecular dynamics; dissipative particle dynamics etc. can be applied and results can be compared.
- Defects like pinhole, crack and waviness can be applied and effect of these defects can be used to measure the change in the young's modulus of elasticity for CNT.
- These defects can also be included in the study of nano-composites and their effect on the properties of composite can be computed.
- The study done in this report is purely analytical and numerical. Till now no significant literature or research is available related to the experimental investigation of various defects in CNT. Experimental validation of above work can be done. This experimental work will require state of art equipments to investigate the faults or even induce one if necessary.

## REFERENCES

- [1] JP Small et al., "Mesoscopic thermal and thermoelectric measurements of individual carbon nanotubes", *Solid State Communications*, 127, pp-181, 2003.
- [2] WA deHeer et al., "A Carbon Nanotube Field-Emission Electron Source", *Science*, 270, pp-1179, 1995.
- [3] MM Treacy et al., "Exceptionally high Young's modulus observed for individual carbon nanotubes", *Nature*, 388, pp-678, 1997.
- [4] EW Wong et al., "Nanobeam Mechanics: Elasticity, Strength, and Toughness of Nanorods and Nanotubes", *Science*, 277, pp-1971, 1997.
- [5] S Iijima, "Helical microtubules of graphitic carbon", *Nature*, 354, pp-56, 1996.
- [6] B Bhushan, "Springer Handbook of Nanotechnology", *Springer*, 2004.
- [7] N Wang et al., "Single-walled 4Å carbon nanotube arrays", *Nature*, 408, pp-50, 2000.
- [8] J Tersoff et al., "Structural properties of a carbon-nanotube crystal", *Physical Review Letters*, 73, pp-676, 1994.
- [9] LX Zheng et al., "Ultralong single-wall carbon nanotubes", *Nature Materials*, 3, pp-673, 2004.
- [10] C Journet et al., "Large-scale production of single-walled carbon nanotubes by the electric-arc technique", *Nature*, 408, pp-756, 1997.
- [11] Y Saito et al., "Growth Conditions of Double-Walled Carbon Nanotubes in Arc Discharge", *Journal of Physical Chemistry B*, 107, pp-931, 2002.
- [12] A Puretzky et al., "Time-resolved diagnostics of single wall carbon nanotube synthesis by laser vaporization", *Applied Surface Science*, 197, pp-552, 2002.
- [13] A Thess et al., "Crystalline Ropes of Metallic Carbon Nanotubes", *Science*, 273, pp-483, 1996.

- [14] KS Choi et al., "The Role of Ammonia Treatment in the Alignment of the Carbon Nanotubes Synthesized with Ni and Fe via Thermal Chemical Vapor Deposition", *Journal of Korean Physical Society*, 39, pp-7, 2001.
- [15] YC Choi et al., "Controlling the diameter, growth rate, and density of vertically aligned carbon nanotubes synthesized by microwave plasma-enhanced chemical vapor deposition", *Applied Physics Letters*, 76, pp-2367, 2000.
- [16] CJ Lee et al., "Synthesis of bamboo-shaped multiwalled carbon nanotubes using thermal chemical vapor deposition", *Chemical Physics Letters*, 323, pp-560, 2000.
- [17] F Rohmund et al., "A simple method for the production of large arrays of aligned carbon nanotubes", *Chemical Physics Letters*, 328, pp-369, 2000.
- [18] OA Nerushev et al., "The temperature dependence of Fe-catalysed growth of carbon nanotubes on silicon substrates", *Physica B*, 323, pp-51, 2002.
- [19] H Ago et al., "Growth of double-wall carbon nanotubes with diameter-controlled iron oxide nanoparticles supported on MgO", *Chemical Physics Letters*, 391, pp-308, 2004.
- [20] JH Hafner et al., "Catalytic growth of single-wall carbon nanotubes from metal particles", *Chemical Physics Letters*, 296, pp-195, 1998.
- [21] S Sato et al., "Carbon nanotube growth from titanium-cobalt bimetallic particles as a catalyst", *Chemical Physics Letters*, 402, pp-149, 2005.
- [22] SN Zaretskiy et al., "Growth of carbon nanotubes from Co nanoparticles and C<sub>2</sub>H<sub>2</sub> by thermal chemical vapor deposition", *Chemical Physics Letters*, 372, pp-300, 2003.
- [23] A Barber et al., "On the tensile strength distribution of multiwalled carbon nanotubes", *Applied Physics Letters*, 87, pp-1, 2005.
- [24] X Zhang et al., "Poly(vinyl alcohol)/SWNT Composite Film", *Nano Letters*, 3, pp-1285, 2003.

- [25] MJ Biercuk et al., "Carbon nanotube composites for thermal management", *Applied Physics Letters*, 80, pp-2767, 2002.
- [26] D Qian et al., "Load transfer and deformation mechanisms in carbon nanotube-polystyrene composites", *Applied Physics Letters*, 76, pp-2868, 2000.
- [27] J Kong et al, "Nanotube Molecular Wires as Chemical Sensors", *Science*, 287, pp-622, 2000.
- [28] JH Hafner et al., "Growth of nanotubes for probe microscopy tips", *Nature*, 398, pp-761, 1999.
- [29] H Dai et al., "Nanotubes as nanoprobe in scanning probe microscopy", *Nature*, 384, pp-147, 1996.
- [30] SS Wong et al., "Covalently functionalized nanotubes as nanometre- sized probes in chemistry and biology", *Nature*, 394, pp-52, 1998.
- [31] P Kim et al., "Nanotube Nanotweezers", *Science*, 286, pp-2148, 1999.
- [32] AM Cassell et al., "Large scale CVD synthesis of single-walled carbon nanotubes", *Journal Physical Chemistry B*, 103, pp-6484, 1999.
- [33] J Kong et al., "Synthesis of individual single-walled carbon nanotubes on patterned silicon wafers", *Nature*, 395, pp-878, 1998.
- [34] P Nikolaev et al., "Gas-phase catalytic growth of single-walled carbon nanotubes from carbon monoxide", *Chemical Physics Letters*, 313, pp-91, 1999.
- [35] K Hata et al., "Water-assisted highly efficient synthesis of impurity-free single-walled carbon nanotubes", *Science*, 306, pp-1362, 2004.
- [36] D Bom et al. , "Thermogravimetric analysis of the oxidation of multiwalled carbon nanotubes: Evidence for the role of defect sites in carbon nanotube chemistry", *Nano Letters*, 2, pp-615, 2002.

- [37] MA Hamon et al., “End-group and defect analysis of soluble single-walled carbon nanotubes”, *Chemical Physics Letters*, 347, pp-8, 2005.
- [38] AC Dillon et al. , “Systematic inclusion of defects in pure carbon single-wall nanotubes and their effect on the Raman D-band”, *Chemical Physics Letters*, 401, pp-522, 2005.
- [39] W Clauss et al. , “Electron backscattering on single-wall carbon nanotubes observed by scanning tunneling microscopy”, *Europhysics Letters*, 47, pp-601, 1999.
- [40] H Kim et al. , “Direct observation of localized defect states in semiconductor nanotube junctions “, *Physical Review Letters*, 90, pp-216107, 2004.
- [41] M Ishigami et al. , “Identifying defects in nanoscale materials”, *Physical Review Letters*, 93, pp-196803, 2004.
- [42] SK Doorn et al., “Raman spectroscopy and imaging of ultralong carbon nanotubes”, *Journal Physical Chemistry B*, 109, pp-3751, 2005.
- [43] Louie, “S. G. in Carbon Nanotubes”, *Springer*, pp-113, 2001.
- [44] Y Fan et al., “Identifying and counting point defects in carbon nanotubes”, *Nature Materials*, 4, pp-906.
- [45] BI Dunlap , “Relating Carbon Tubules”, *Physical Review B*, 49, pp-5643, 1994.
- [46] ZH Zhu et al., “Molecular Orbital Theory Calculations of the H<sub>2</sub>O-Carbon Reaction”, *Energy & Fuels*, 16, pp-847, 2002.
- [47] SL Mielke et al., “The Role of Vacancy Defects and Holes in the Fracture of Carbon Nanotubes”, *Chemical Physics Letters*, 390, pp-413, 2004.
- [48] Q Zhao et al., *Physical Review B*, 65, pp-144105, 2004.
- [49] VH Crespi et al., *Physical Review Letters*, 79, pp-2093, 1997.
- [50] V Gayathri et al., “Carbon nanotube as NEMS sensor – effect of chirality and stone-wales defect intend”, *Journal of Physics*, 34, pp-824, 2006.

- [51] FT Fisher et al., "Fiber waviness in nanotubereinforced polymer composites - I: modulus predictions using effective nanotube properties", *Composites Science and Technology*, 63, pp-1689, 2003.
- [52] RD Bradshaw et al., "Fiber waviness in nanotubereinforced polymer composites - II: modeling via numerical approximation of the dilute strain concentration tensor", *Composites Science and Technology*, 63, pp-1705, 2003.
- [53] RF Gibson et al., "A comprehensive closed form micromechanics model for estimating the elastic modulus of nanotubereinforced composites", *Composites Part A*, 37, pp-2178, 2006.
- [54] R Andrews et al., "Fabrication of carbon multiwall nanotube/polymer composites by shear mixing", *Macromol Mater Eng*, 287, pp-395, 2002.
- [55] L Berhan et al., "Effect of nanorope waviness on the effective moduli of nanotube sheets", *Journal of Applied Physics*, 95(9), 2004.
- [56] FT Fisher et al., "Effects of nanotube waviness on the modulus of nanotube-reinforced polymers", *Applied Physics Letters*, 80, pp-24, 2004.
- [57] ZL Wang et al., "Nanomeasurements of individual carbon nanotubes by in situ TEM", *Pure Applied Chemistry*, 72(1-2), pp-209, 2000.
- [58] R Gao et al., "Nanomechanics of Individual Carbon Nanotubes from Pyrolytically Grown Arrays", *Physical Review Letters*, 85(3), 2000.
- [59] ZL Wang et al., "Mechanical and electrostatic properties of carbon nanotubes and nanowires", *Materials Science & Engineering C*, 16, pp-3, 2001.
- [60] B Kang et al., "Free vibration analysis of planar curved beams by wave propagation", *Journal of Sound and Vibration*, 260, pp-19, 2003.
- [61] TW Ebbesen et al., "Topological and sp<sup>3</sup> defect structures in Nanotubes", *Carbon*, 33, pp-937, 1995.



- [62] KI Tserpes et al., "The effect of Stone–Wales defect on the tensile behavior and fracture of single-walled carbon nanotubes", *Composite Structures*, 79, pp-581, 2007.
- [63] N Chandra et al., "Local elastic properties of carbon nanotubes in the presence of Stone–Wales defects", *Physical Review B*, 69, pp-964101, 2004.
- [64] M Pirmoradian et al., "Effect of Vacancy Defects on the Fundamental Frequency of Carbon Nanotubes", *International Conference on Nano/Micro Engineered and Molecular System*, 2008.
- [65] Y Hirai et al., "Molecular Dynamics Studies on Mechanical Properties of Carbon Nano Tubes with Pinhole Defects", *Japanese Journal of Applied Physics*, 42, pp-4120, 2003.
- [66] T Belytschko et al., "Atomistic simulations of nanotube fracture", *Physical Review B*, 65, pp-235430, 2002.
- [67] KM Liew et al., "On the study of elastic and plastic properties of multi-walled carbon nanotubes under axial tension using molecular dynamics simulations", *Acta Materiala*, 52, pp-2521, 2004.
- [68] C Li et al., "A structural mechanics approach for the analysis of carbon nanotubes", *International Journal of Solids Structures*, 40, pp-2487, 2003.
- [69] KI Tserpes et al., "Finite element modeling of single-walled carbon nanotubes", *Compos Part B Eng*, 36, pp-468, 2005.
- [70] DW Brenner et al., "Empirical potential for hydrocarbons for use in simulating the chemical vapor deposition of diamond films", *Physical Review B*, 42(15), pp-9458, 1990.
- [71] DW Brenner et al., "A second-generation reactive empirical bond order (rebo) potential energy expression for hydrocarbons", *Journal of Physics, Condensed Matter*, 14(4), pp-783, 2002.

- [72] NL Allinger et al., "Molecular mechanics. the mm3 force field for hydrocarbon", *Journal of the American Chemical Society*, 111(23), pp-8551, 1989.
- [73] FL Darkrim et al., "Review of hydrogen storage by adsorption in carbon nanotubes", *International Journal of Hydrogen Energy*, 27(2), pp-193, 2002.
- [74] T Hertel et al., "Deformation of carbon nanotubes by surface van der waals forces", *Physical Review B*, 58(20), pp-13870, 1998.
- [75] S Iijima et al., "Structural flexibility of carbon nanotubes", *Journal of Chemical Physics*, 104, pp-2089, 1996.
- [76] A Sears et al., "Buckling of multiwalled carbon nanotubes under axial compression", *Physical Review B*, 73(8), pp-85410, 2006.
- [77] F Ding et al., "Pseudoclimb and dislocation dynamics in superplastic nanotubes", *Physical Review Letters*, 98(7), pp-75503, 2007.
- [78] CL Zhang et al., "Self-healing in defective carbon nanotubes: A molecular dynamics study", *Journal of Physics, Condensed Matter*, 19(38), pp-386212, 2007.
- [79] Hod, et al., "Carbon nanotube closed-ring structures", *Physical Review B*, 67(19), pp-195497, 2003.
- [80] J Gavillet et al., "Root-growth mechanism for single-wall carbon nanotubes", *Physical Review Letters*, 87(27), pp-275504, 2001.
- [81] AN Kolmogorov et al., "Nanotube-substrate interactions: Distinguishing carbon nanotubes by the helical angle", *Physical Review Letters*, 92(8), pp-85503, 2004.
- [82] BI Yakobson et al., "Nanomechanics of carbon tubes: Instabilities beyond linear response", *Physical Review Letters*, 76(14), pp-2511, 1996.
- [83] A Sears et al., "Macroscopic properties of carbon nanotubes from molecular-mechanics simulations", *Physical Review B*, 69(23), pp-235406, 2004.

- [84] W Yu et al., "Atomistic simulation of the torsion deformation of carbon nanotubes", *Modelling and Simulation in Materials Science and Engineering*, 12(6), pp-1099, 2004.
- [85] M Dequesnes et al., "Calculation of pull-in voltages for carbon-nanotube-based nanoelectromechanical switches", *Nanotechnology*, 13(1), pp-120, 2002.
- [86] M Dequesnes et al., "Static and dynamic analysis of carbon nanotube-based switches", *Journal of Engineering Materials and Technology*, 126, pp-230, 2004.
- [87] C Li et al., "Single-walled carbon nanotubes as ultrahigh frequency nanomechanical resonators", *Physical Review B*, 68(7), pp-73405, 2003.
- [88] C Li et al., "Vibrational behaviors of multiwalled-carbonnanotube-based nanomechanical resonators", *Applied Physics Letters*, 84, pp-121, 2003.
- [89] C Li et al., "Mass detection using carbon nanotube-based nanomechanical resonators", *Applied Physics Letters*, 84, pp-5246, 2004.
- [90] H Jiang et al., "Intrinsic energy loss mechanisms in a cantilevered carbon nanotube beam oscillator", *Physical Review Letters*, 93(18), pp-185501, 2004.
- [91] PJ Hoogerbrugge et al., "Simulating microscopic hydrodynamic phenomena with dissipative particle dynamics", *Europhysics Letters*, 19(3), pp-155, 1992.
- [92] A Maiti et al., "Nanotube-polymer composites: Insights from flory-huggins theory and mesoscale simulations", *Molecular Simulation*, 31(2-3), pp-143, 2005.
- [93] D Qian et al., "Mechanics of carbon nanotubes", *Applied Mechanics Reviews*, 55, pp-495, 2002.
- [94] EB Tadmor et al., "Quasicontinuum analysis of defects in solids", *Philosophical Magazine A*, 73(6), pp-1529, 1996.
- [95] T Belytschko et al., "Continuum mechanics modeling and simulation of carbon nanotubes", *Meccanica*, 40(4), pp-455, 2005.

- [96] T Belytschko et al., "Nonlinear mechanical response and rippling of thick multiwalled carbon nanotubes", *Physical Review Letters*, 91(21), pp-215505, 2003.
- [97] GM Odegard et al., "Equivalent continuum modeling of nano-structured materials", *Composites Science and Technology*, 62(14), pp-1869, 2002.
- [98] XY Wang et al., "Numerical simulation for bending modulus of carbon nanotubes and some explanations for experiment", *Composites Part B*, 35(2), pp-79, 2004.
- [99] LV Zhigilei et al., "Mesoscopic model for dynamic simulations of carbon nanotubes", *Physical Review B*, 71(16), pp-165417, 2005.
- [100] S Xiao et al., "Studies of nanotube-based resonant oscillators through multiscale modeling and simulation", *Physical Review B*, 75(12), pp-125414, 2007.
- [101] T Belytschko et al., "Coupling methods for continuum model with molecular model", *International Journal for Multiscale Computational Engineering*, 1(1), pp-115, 2003.
- [102] JP Lu et al., "Elastic properties of carbon nanotubes and nanoropes", *Physical Review Letters*, 79(7), pp-1297, 1997.
- [103] JA Pelesko et al., "Modeling MEMS and NEMS", Chapman & Hall/CRC, 2003.
- [104] V Sazonova et al., "A tunable carbon nanotube electromechanical oscillator", *Nature*, 431, pp-287, 2004.
- [105] YW Kwon et al., "Vibrational characteristics of carbon nanotubes as nanomechanical resonators", *Journal Nanoscience & Nanotechnology*, 5(5), pp-703, 2005.
- [106] Q Zheng et al., "Multiwalled carbon nanotubes as gigahertz oscillators", *Physical Review Letters*, 88(4), pp-45503, 2002.
- [107] Q Zheng et al., "Excess van der Waals interaction energy of a multiwalled carbon nanotube with an extruded core and the induced core oscillation", *Physical Review B*, 65(24), pp-245409, 2002.

- [108] P Liu et al., "Oscillatory behavior of gigahertz oscillators based on multiwalled carbon nanotubes", *Journal of Applied Physics*, 98, pp-14301, 2005.
- [109] K Schwab et al., "Spring constant and damping constant tuning of nanomechanical resonators using a single-electron transistor", *Applied Physics Letters*, 80(7), pp-1276, 2002.
- [110] B Reulet et al., "Acoustoelectric effects in carbon nanotubes", *Physical Review Letters*, 85(13), pp-2829, 2000.
- [111] JF Davis et al., "High-Q mechanical resonator arrays based on carbon nanotubes", *Third IEEE conference on nanotechnology*, 2, pp-635, 2003.
- [112] NA Prokudina et al., "A carbon nanotube film as a radio frequency filter", *Carbon*, 43, pp-1815, 2005.
- [113] Mathematica, Wolfram Research, Inc.
- [114] ZL Wang et al., "Measuring physical and mechanical properties of individual carbon nanotubes by in situ TEM", *Journal of Physics Chemistry & Solids*, 61, pp-1025, 2000.
- [115] BY Wei et al., "Examining the gas-sensing behaviors of carbon nanotubes using a piezoelectric quartz microbalance", *Sensors Mater*, 15(4), pp-177, 2003.
- [116] S Chopra et al., "Selective gas detection using a carbon nanotube sensor", *Applied Physics Letters*, 83(11), pp-2280, 2003.
- [117] S Chopra et al., "Carbon nanotube-based resonant circuit sensor for ammonia", *Applied Physics Letters*, 80(24), pp-4632, 2002.
- [118] M Grujicic et al., "A computational analysis of the carbon nanotube-based resonant circuit sensors", *Applied Surface Science*, 229(1-4), pp-316, 2004.
- [119] AY Joshi et al., "Vibration Analysis of Prestressed Single Walled CNT based Mass sensors", *International Journal of Electropun nanofibers and applications*, 2(3), pp-161, 2008.

- [120] AY Joshi et al., "Vibration Signature Analysis of Single Walled Carbon Nanotube Based Nano Mechanical Sensors", *Physica E*, 42(8), pp-2115, 2010.
- [121] K Jensen et al., "An atomic-resolution nanomechanical mass sensor", *Nature Nanotechnology*, 3, pp-533, 2008.
- [122] XD Han et al., "Low-temperature in situ large-strain plasticity of silicon nanowires", *Advanced Materials*, 19(16), pp-2112, 2007.
- [123] T Belytschko et al., "Coupled quantum mechanical/molecular mechanical modeling of the fracture of defective carbon nanotubes and graphene sheets", *Physical Review B*, 75(7), pp-75412, 2007.
- [124] C Li et al., "Measurement of the elastic properties and intrinsic strength of monolayer graphene", *Science*, 321, pp-385, 2008.
- [125] B Peng et al., "Measurements of near-ultimate strength for multiwalled carbon nanotubes and irradiation-induced crosslinking improvements", *Nature Nanotechnology*, 3, pp-626, 2008.
- [126] NM Pugno et al., "Quantized fracture mechanics", *Philosophical Magazine*, 84(27), pp-2829, 2004.
- [127] MF Yu et al., "Strength and breaking mechanism of multiwalled carbon nanotubes under tensile load", *Science*, 287, pp-637, 2000.
- [128] T Belytschko et al., "Mechanics of defects in carbon nanotubes: atomistic and multiscale simulations", *Physical Review B*, 71(11), pp-115403, 2005.
- [129] F Celarie et al., "Glass breaks like metal, but at the nanometer scale", *Physical Review Letters*, 90(7), pp-75504, 2003.
- [130] HJ Gao et al., "Materials become insensitive to flaws at nanoscale: lessons from nature", *Proceedings of the National Academy of Sciences USA*, 100(10), pp-5597, 2003.

- [131] JP Guin et al., "Fracture of silicate glasses: ductile or brittle?", *Physical Review Letters*, 92(21), pp-215502, 2004.
- [132] T Belytschko et al., "Nanoscale fracture mechanics", *Annual Review of Physical Chemistry*, 58, pp-185, 2007.
- [133] RO Ritchie et al., "Characteristic dimensions and the micro-mechanisms of fracture and fatigue in 'nano' and 'bio' materials", *International Journal of Fracture*, 128(1-4), pp-1, 2004.
- [134] BI Jakobson et al., *Journal of Computational Material Science*, 8, pp-341, 1997.
- [135] MB Nardelli et al., *Journal of Physical Review B*, 57, pp-4277, 1998.
- [136] S Mohammadi, "Extended Finite Element Method for fracture analysis of structures", Blackwell Publishing Ltd, 2008.
- [137] G Irwin, "Analysis of stresses and strains near the end of a crack traversing a plate", *Journal of Applied Mechanics*, 1957.
- [138] DM Parks, "The Virtual Crack Extension Method for Nonlinear Material Behavior", *Computer Methods in Applied Mechanics and Engineering*, 12, pp-353, 1977.
- [139] CF Shih et al., "Energy Release Rate along a Three-Dimensional Crack Front in a Thermally Stressed Body", *International Journal of Fracture*, 30, pp-79, 1986.

## LIST OF PUBLICATION

---

### INTERNATIONAL JOURNALS:

1. Anand Y. Joshi, **Aashish Bhatnagar**, S.P. Harsha and Satish C. Sharma, “Vibratory Analysis of a Doubly Clamped Wavy Single Walled Carbon Nanotube based Nano Mechanical Sensors”, *International Journal of Engineering Science and Technology*, **2(5)**, pp-993, 2010. Impact Factor – **1.85**
2. Anand Y. Joshi, **Aashish Bhatnagar**, S.P. Harsha and Satish C. Sharma, “Vibration Response Analysis of Doubly Clamped Single Walled Wavy Carbon Nanotube Based Nanomechanical Sensors”, *Transaction of ASME - Journal of Nanotechnology in Engineering and Medicine*, **Accepted**.
3. **Aashish Bhatnagar**, Anand Y. Joshi, S.P. Harsha and Satish C. Sharma, “An investigation of mass sensitivity of fixed free single walled carbon nanotube based Nano mechanical sensors”, *Current Nanoscience*, **Communicated**. Impact Factor – **1.47**.
4. **Aashish Bhatnagar**, Anand Y. Joshi, S.P. Harsha and Satish C. Sharma, “The effect of pinhole defects on vibrational characteristics of single walled carbon nanotube”, *Physica E*, **Communicated**. Impact Factor – **1.23**.
5. **Aashish Bhatnagar**, Anand Y. Joshi, S.P. Harsha and Satish C. Sharma, “Analysis of crack propagation in single walled carbon nanotube subjected to tensile loading”, *Computer Modelling in Engineering and Sciences*, **Communicated**. Impact Factor – **4.7**.



## INTERNATIONAL CONFERENCES:

1. **Aashish Bhatnagar**, P.K. Kankar, S.P. Harsha And Satish C. Sharma, “ANN Based Fault Classification of High Speed Ball Bearings” *Proceedings of The ASME International Design Engineering Technical Conferences & Computers And Computers And Information In Engineering Conference IDETC/CIE 2009*, August 30-September 2, 2009, San Diego, California, USA.
2. P. K. Kankar, Kalyan Manohar B, **Aashish Bhatnagar**, Satish C. Sharma And S. P. Harsha, “Vibration Based Fault Diagnosis of Rolling Element Bearings using Artificial Neural Networks And Support Vector Machines”, *2nd Conference on Dynamics, Vibration and Control*, August 10-15, 2009, Chengdu, Sichuan, China.